PROTON-PROTON ELASTIC SCATTERING
AND NUCLEON RESONANCE PRODUCTION AT HIGH ENERGIES

J.V. ALLABY, A.N. DIDDENS, R.W. DOBINSON, A. KLOVNING[†], J. LITT,
L.S. ROCHESTER[††], K. SCHLÜPMANN[†††] and A.M. WETHERELL
CERN, Geneva, Switzerland

U. AMALDI, R. BIANCASTELLI, C. BOSIO and G. MATTHIAE
Physics Laboratory, Istituto Superiore di Sanita and INFN, Sezione Sanita, Rome, Italy

Abstract Angular distributions of proton-proton elastic scattering have been measured for in-
cident beam momenta of 10.0, 12.0, 14.2 and 24.0 GeV/c over a range of lab scattering
angles from 12 to 152 mrad. This is equivalent to a range of four-momentum transfer
squared from about 0.1 to 6.7 GeV² at the highest momentum. Nucleon resonance pro-
duction in the two-body reaction p + p → p + X has been studied at 24.0 GeV/c incident
momentum from 13.5 to 112 mrad by measuring the proton momentum spectra from
the elastic peak down to a momentum corresponding to a missing mass of about 2.6 GeV.
The new data are compared with previous results and theoretical models.

1. Introduction

Since the advent of multi-GeV proton accelerators large numbers of experimen-
tal studies of elastic proton-proton scattering have been made. In addition, a con-
siderable amount of information on the simplest two-body inelastic pp reactions,
p + p → p + X (where X denotes a nucleon resonance), has been gathered. As a re-
sult, the *general* features of these basic proton reactions are well-known up to
about 30 GeV/c incident proton momentum, but the *detailed* features of the angu-
lar distributions, particularly at higher momenta above say 10 GeV/c, are poorly
known. It may be added that pp elastic scattering has been measured at the highest
momentum transfer of any hadron-hadron reaction studied because of the high in-
tensity and good optical quality of proton beams.

The purpose of the present experiment was to study angular distributions in
detail over a large range of momentum transfer and with high accuracy. With this

---

object in view a high-resolution, single-arm, magnetic spectrometer was employed. The results obtained comprise angular distributions of elastic scattering for incident proton momenta of 10.0, 12.0, 14.2 and 24.0 GeV/c over a range of lab scattering angles from 12 to 152 mrad. This is equivalent to a range of four-momentum transfer squared from about 0.1 to 6.7 GeV^2 at the highest momentum. Some data were also taken at an incident momentum of 19.2 GeV/c to overlap with earlier measurements [1]. Nucleon resonance production was studied at 24 0 GeV/c over a range of four-momentum transfer squared from about 0.1 to 6.4 GeV^2. Preliminary values of both elastic [2] and nucleon resonance production [3] data from this experiment have been already published. In the present paper the final results will be collated with previous experimental data, the aim being to present as complete a picture as possible of the situation up to 30 GeV/c.

The contents of the paper are arranged as follows subsects. 2.1, 2.2 and 2.3 give an account of the available experimental data on pp elastic scattering and in subsect. 2.4 a brief résumé of the various theoretical models used to describe elastic scattering is given. The present experimental status of single nucleon resonance production is discussed in subsect. 2.5 together with a brief review of theoretical models. In sect. 3 the experimental technique is described and in sect. 4 the method of data analysis and the results are presented. Sect. 5 gives a discussion of the results on both elastic and inelastic scattering together with a comparison with theoretical models, and sect. 6 presents the conclusions of the experiment in the light of other results.

2. General discussion of the present status of high-energy proton-proton scattering experiments

2.1. Elastic proton-proton scattering - general remarks

The most striking feature of high-energy proton-proton elastic scattering, in common with the other hadronic systems, is the division of the angular distribution into two rather distinct regions of momentum transfer. The regions may be characterized, qualitatively, as follows

(i) There is a sharp forward peak, which may be described by

$$\frac{d\sigma}{dt} \sim \exp\left(-b|t| + ct^2\right),\tag{1}$$

where $|t|$ is the square of the four-momentum transfer and b and c are parameters ($b \simeq 10$ GeV^{-2} and $c \simeq 2$ GeV^{-4} around 15 GeV/c). Relation (1) is valid for $|t| \lesssim 1$ GeV^2. This part of the angular distribution is weakly energy dependent or, in other words, the parameters b and c vary slightly with energy, the angular distribution thereby shrinking. The forward peak is generally recognised [4] to be a diffraction or shadow scattering phenomenon caused by the absorptive processes

(comprising about 30 mb out of a total cross section of about 40 mb) in high-energy pp collisions As a result, the forward scattering amplitude is mainly imaginary.

(ii) For $|t| \gtrsim 1$ GeV^2 the angular distributions are much flatter than described by eq. (1), being qualitatively of the form $\sim \exp -(b'\sqrt{|t|})$, and have a very strong energy-dependence. There is no general agreement about the scattering mechanism in this region. Thus, for this reason and because of the lack of accurate experimental data, the experiment presented in this paper concentrated upon this momentum transfer region.

The description of elastic scattering which follows is based upon the crude division contained above in points (i) and (ii). This is not to say that any profound physical significance should be attached to such a division, rather it proves to be a convenient means of presentation.

2.2. Elastic proton-proton scattering in the diffraction region ($|t| \lesssim 1$ GeV^2)

The experimental information [5] collected in the diffraction region is considerable, and the shape parameters b and c of formula (1) are reasonably well determined up to 30 GeV/c incident proton momentum, by fitting over a $|t|$ range up to 1 GeV^2. For a sufficiently small range of $|t|$ formula (1) is obviously well approximated by

$$\frac{d\sigma}{dt} \sim \exp(-b|t|). \tag{2}$$

In the simplest optical model description [6] of diffraction scattering the parameter b, measured as $|t| \to 0$, is proportional to the square of the proton radius. The essential energy-dependence or shrinking of the diffraction peak is characterised by the increase of b with energy. Measurements [7], for $|t| \lesssim 0.1$ GeV^2, show that the shrinkage continues up to 70 GeV in a manner compatible with a logarithmic energy-dependence. Furthermore, results [8] obtained at the CERN Intersecting Storage Rings (ISR) indicate that the shrinkage extends into the region of several hundred to above one thousand GeV Recent measurements [9] at the ISR, for energies equivalent to 500- 1500 GeV, show that formula (2) is not a good representation of the differential cross section over the range $0 \lesssim |t| \lesssim 0.2$ GeV^2. In fact, there is a "break" in the angular distribution around $|t| \sim 0.1$ GeV^2 and formula (2), with an appropriate value of b, gives a good description of the data below this momentum transfer. This structure was indeed suggested by the data up to 30 GeV/c, as pointed out by Carrigan [10], however the details of the angular distributions up to $|t| \simeq 0.2$ GeV^2 are not yet well-known in this momentum range.

2.3. Elastic proton-proton scattering at moderate and large momentum transfers ($|t| \gtrsim 1$ GeV^2)

Experiments to measure complete angular distributions in detail for $|t| \gtrsim 1$ GeV^2 have been little performed at proton momenta above 7 GeV/c. Reasons for this

are that the cross sections become very small and that large ranges of momentum transfer must be covered; for example, the momentum transfer for $90°$ scattering at 30 GeV/c corresponds to $|t| = 27.2$ GeV^2.

Early measurements of high-energy pp scattering for $|t| \gtrsim 1$ GeV^2 were performed at CERN [11] and at Brookhaven [12] The data collected, although rather sparse and not very precise, did indicate the rough general features as described by point (ii) in subsect. 2.1 above. In particular, they showed the very rapid decrease with energy of the cross section at fixed momentum transfer. A simple parametrisation representing the rapid decrease was suggested by Orear [13] who showed that, within errors, the differential cross section at large momentum transfers could be written

$$s \frac{d\sigma}{d\Omega} = A \exp(p_T/a) , \tag{3}$$

where s is the square of the c.m. energy, $d\sigma/d\Omega$ is the c.m. differential cross section, and p_T is the transverse momentum $p \sin \theta$.

In the Orear fit the constant a was 158 ± 3 MeV/c. This formula was found to hold within the rather large experimental errors over a range of p_T from 0.8 to 4.0 GeV/c and for data covering incident momenta from 1.7 up to 30 GeV/c. In addition, the same parametrisation, differing only in the coefficient A, was found [13] to fit the available data on the inelastic reaction $p + p \rightarrow \pi^+ + d$.

The exponential dependence on the transverse momentum indicated by eq. (3) led to an attempt to understand the physics of large momentum transfer scattering in terms of a specific model, the "statistical" or "thermodynamic" model of Hagedorn [14]. Indeed, the coefficient a as determined by the Orear parametrisation seemed to be numerically very close to its analogue (the maximum temperature) in the thermodynamic model. In addition the experimental results of Ankenbrandt et al. [15] on the production of nucleon resonances at large momentum transfers in proton-proton collisions could also be interpreted from a statistical or thermodynamical point of view, since the cross sections were found to be of the same order and to behave in a similar manner to those for pp elastic scattering.

The thermodynamic model of Hagedorn could give only a qualitative prediction that the differential cross section near $90°$ should fall as an exponential in transverse momentum, with a slope of about the value found experimentally, and no information about the angular distribution. However, other statistical model considerations by Ericson [16] gave specific predictions on the angular distribution, by analogy with the situation in low-energy nuclear reactions. Because of the random nature of the partial-wave scattering amplitudes in a statistical model, Ericson predicted that the angular distribution at fixed energy should show a characteristic structure in the form of fluctuations Such fluctuations had indeed been observed in nuclear reactions in the 10 MeV range.

An experiment designed to search for these fluctuations was carried out by Allaby et al. [17] who measured the angular distribution for pp elastic scattering at

16.9 GeV/c incident momentum over the c.m. angular range $67°$ to $90°$. No fluctuations were found, which led to a discarding of the strictly statistical interpretation of large momentum transfer scattering. In addition, this experiment showed an exponential fall-off with $p_\perp$, but with a different coefficient from the "universal" slope of the Orear fit. The value of a from the new experiment was 225 ± 4 MeV/c.

This result led to an extension [18] of the measurements over a range of incident momenta from 8.1 to 21.3 GeV/c to determine the momentum-dependence of the parameter a in the angular region $67°$ $90°$. The parameter a was found to change abruptly from a value of 160 MeV/c to 230 MeV/c at an incident momentum of ~ 10 GeV/c.

Related experiments were carried out by Akerlof et al. [19] who measured the differential cross section at $90°$ c.m. angle at many momenta between 5.0 and 13.4 GeV/c. The discontinuity in the parameter a was reflected by a sharp change in the rate of decrease of the differential cross section at $90°$ as a function of incident momentum. In fact, when the results were plotted in the form of $\ln(d\sigma/dt)_{90°}$ against $p_{c.m.}^2$, they were found to lie on two straight lines intersecting at a value of $p_{c.m.}^2$, corresponding to a lab momentum of 8 GeV/c.

Since this interesting phenomenon seemed to appear in the region of 8 GeV/c incident momentum, further measurements were made [20] in the range 7 to 12 GeV/c in order to study the angular distribution over the range $40°$ $90°$ c.m.. The results suggested that the "break", or change of exponential slope of the angular distribution, was the reflection of an unsuspected structure which seemed to appear at incident momenta above 8 GeV/c and at a value of the four-momentum transfer squared $|t| \approx 1.5$ GeV^2. Unfortunately the data did not extend to small enough angles to permit a definite conclusion, also any interpretation relied on linking up these data points with older results on elastic pp scattering in the diffraction region.

Thus it seemed desirable to extend these measurements over a wide angular range. Using a high-resolution, single-arm spectrometer, the angular distributions for elastic pp scattering were measured at CERN [1] over the range $0.1 < |t| < 6.0$ GeV^2 at 19.2 GeV/c incident momentum and $0.1 < |t| < 1.9$ GeV^2 at 21.1 GeV/c. These elastic distributions gave striking confirmation of the structure at $|t| \approx 1.5$ GeV^2 suggested by the previous measurements. The present experiment provides further information on this point between 10 and 24 GeV/c.

2.4. Elastic scattering - theoretical approaches

A large amount of theoretical work [21] has been done on elastic proton-proton scattering and the following does not aim to give a comprehensive survey, rather the most intensively pursued models or approaches will be listed and briefly described in order to provide a background for comparison with the data.

2.4.1. Thermodynamic or statistical model

The purely thermodynamic or statistical model, which has already been mentioned in subsect. 2.3, has been rediscussed by Frautschi [22] who suggested that a necessary condition for the generation of Ericson fluctuations is the presence of direct channel resonances in the scattering system. As the pp system possesses no direct channel resonances, the experimental absence [17] of fluctuations cannot then be used as a proof of a non-statistical behaviour in large-angle pp scattering. This question may therefore be considered to be still open.

2.4.2. Diffraction or shadow scattering models

The physical idea that high-energy elastic scattering is essentially shadow scattering resulting from the absorption of the incident waves by the many open interaction channels has been turned into a formal diffraction model by Van Hove [4]. The use of a particular "ansatz" for the overlap function describing the contribution of all inelastic final states to the unitarity condition for elastic scattering leads to a form for the diffraction peak of the type given by formula (1) in subsect. 2.1, and to the correct ratio of elastic to total cross sections. This approach has also been employed in an attempt to understand the origin of the "break" at 8 GeV/c described above in subsect. 2.3. It was pointed out [18] that the baryon pair production processes near threshold should have reactive effects on the low partial waves of elastic scattering, thus modifying the angular distribution at large angles. A unitarity calculation along these lines by Kokkedee and Van Hove [23] indicated that the total baryon pair production cross section around 10 GeV/c was of the right order of magnitude to explain the change of slope at 8 GeV/c.

The diffraction model of Krisch [24, 25] also relates elastic scattering to production processes. Using all the data available up to 1967, Krisch found that the formula

$$\frac{d\sigma}{dt} = \sum_{i=1}^{3} c_i \exp\left(-\beta^2 p_T^2 / g_i\right).$$ (4)

where c_i, g_i are parameters, β is the c.m. proton velocity and p_T is the transverse momentum, gave a rather impressive fit over 12 orders of magnitude of the cross section. The fact that three regions appeared which were exponential in the variable $\beta^2 p_T^2$ was interpreted as being the result of diffraction scattering associated with three different types of inelastic processes namely pion production, kaon production and anti-proton production. In other words, proton scattering should be understood in terms of shadow scattering from three distinct spatial regions. Subsequent more accurate data do not fall on the dependence (4). In particular the data in the region of the structure, at $|t|$ values ~ 1.5 GeV^2, fall well below the suggested parametrization. Hence the simple and attractive features of the model are rendered invalid. Furthermore, experiments [26] on inelastic processes, performed specifically to test the model, have given negative results.

Finally, in this context, it is worth noting suggestions [27] that the variable $\beta^2 p_1^2$ for elastic scattering is a special case of a more general variable of use in discussing scattering processes and in particular at small momentum transfers.

2.4.3. Optical models

As shadow scattering is evidently an important element in elastic processes the description by a Fraunhofer diffraction optical model is clearly indicated. The mathematical formulation is well defined and the physical input consists essentially of a postulated matter density distribution. An early attempt in this direction was made by Serber [28] who tried to reproduce the t-dependence of the data of refs. [11, 12] using a matter density distribution obtained by superimposing a Yukawa and a Gaussian shape. The model did not represent the situation very well, particularly with the advent of later data of higher accuracy

With regard to the question of the matter density distribution, Wu and Yang [29] made a suggestion which connected elastic pp differential scattering cross sections with the fourth power of the proton electromagnetic form factor This effectively identifies the proton matter distribution with the electromagnetic charge distribution, as determined by electron-proton scattering Taking into account this idea and considering protons as extended nuclear matter distributions, determined by the electromagnetic form factor, optical models [30] have been used to calculate an elastic scattering angular distribution which is supposed to hold at asymptotic energies This latter point is an interesting suggestion, as it indicates that the limiting or asymptotic behaviour can be predicted from information already available. It is typical of these models that they predict sharp diffraction zeros, the positions being determined by the detailed shape of the density distribution

The observed structure in the angular distribution, described in subsect. 2.3, bears a qualitative resemblance to that of the optical models but, as such models are valid only at asymptotic energies, the observed energy dependence cannot be discussed within this context. Additional energy-dependent amplitudes have to be included to give a reasonable description of the data Indeed some optical models merely use the formalism as a framework to provide a fit to the data using energy-dependent amplitudes

2.4.4. Multiple scattering models

Results [31] similar to those from the optical models have been obtained by considering the proton as made up of a large or small number of constituents, or more specifically of quarks, and performing the calculation of the cross section in terms of the multiple scattering formalism of Glauber [32]. In fact a formal connection exists between the optical models [30] and the multiple scattering method. The higher-order diffraction minima of the optical models appear in the Glauber method as interference between different orders of scattering (single and double, or double and triple scattering, etc.). For increasing momentum transfer, higher-order scattering processes become more important with respect to single scattering Con-

sequently, a possibility underlined by this approach is that there is no true high momentum transfer elastic scattering, rather that large transverse momenta are built up in a series of steps and not generated in one localised deflection.

In the framework of a multiple scattering description, a particularly lucid discussion has been given by Cocconi [33] who related the transverse momentum dependence which is essentially Gaussian in behaviour at small angles [eq. (2)] to the exponential behaviour at large angles [eq. (3)].

2.4.5. Models involving Regge singularities

It has been hoped that Regge theories would provide a dynamical basis for strong interactions and in particular of hadronic elastic scattering. Such an ambitious programme is very far from being achieved, and may indeed be impossible to accomplish, nevertheless a useful phenomenology has emerged on the basis of this theory. In the following, some of the Regge approaches to elastic proton-proton scattering will be briefly listed.

Conventional Regge-pole theory has been repreatedly used [34] to describe scattering at small and at intermediate momentum transfers. Such models generally involve the exchange of at least three trajectories, in particular the P, P' and ω. The approach is such that the number of independent adjustable parameters is large and consequently good fits to the data can be obtained

While the normal Regge-pole calculations would be generally considered to apply for small to moderate momentum transfers, it has been noted [35] that other singularities in the complex angular momentum plane, namely branch points or cuts, should play an important role, particularly at large momentum transfers Consequently models involving both poles and cuts have been used to discuss the data The "hybrid" model of Chiu and Finkelstein [36] is an interesting attempt in this direction. An amplitude containing both poles and cuts is constructed from a part corresponding to the asymptotic limit of Chou and Yang (effectively a fixed Pomeranchuk pole) and a part consisting of normal moving Regge trajectories. The latter introduces an energy dependence which becomes asymptotically zero, the need for which was noted above in subsect. 2.4.3.

An approach related to the original work of Anselm and Dyatlov [35] has been made by Frautschi and Margolis [37] who employed a Glauber-like multiple scattering formalism to generate multiple exchange corrections in a model employing a moving Pomeranchuk pole At energies in the 20 GeV region, both the Chiu-Finkelstein and Frautschi-Margolis models give qualitatively similar results. At considerably higher energies however the Chiu-Finkelstein cross section approaches the Chou-Yang asymptotic limit while the Frautschi-Margolis calculation predicts a cross section which decreases drastically with energy, essentially because of the typical energy-dependence of a normal (moving) Regge-pole.

Other [38] pole and cut models with specific forms for the singularities, for example a Veneziano representation [39], have been worked out

In a rather different approach it has been suggested [40] that the pp scattering

amplitude is composed of two parts, one being a diffractive tail which falls very rap-
idly for fixed t as the energy is increased, and the other a point interaction of cur-
rent-current form which depends on t alone. As the energy in the scattering process
is increased the contact term eventually dominates. In this model the energy-depen-
dent part of the amplitude is provided by a normal Regge pole term. The contact
interaction, of vector form, is concerned with the same current whose transition
form factors are measured in weak and electromagnetic processes. A calculation
satisfying unitarity yields a smooth, structureless angular distribution, not too far
in overall cross section from the data around 25 GeV. While the absence of struc-
ture may be considered as a defect of this model, the interpretation of large-t, high
energy pp scattering in terms of a fundamental point-like interaction remains an
interesting suggestion.

2.4.6. General properties of the scattering amplitude

The strong energy-dependence of the large-angle differential cross section, de-
scribed roughly by eq. (3), has been discussed in connection with the general prop-
erties of the elastic scattering amplitude. It may be shown [41,42], from analyticity
and unitarity, that there is a lower bound for the elastic amplitude at fixed (large)
angle which is given by

$$f(s, \theta) \geqslant K \exp\{-c(\theta) s^{\gamma} \ln s\}\tag{5}$$

where $c(\theta)$ and γ are positive, and K is a constant. The original work of Cerulus and
Martin [41] gave $\gamma = \frac{1}{2}$, whereas a later discussion [42] involving a linearly rising
Regge trajectory gave $\gamma = 1$. The large momentum transfer data available violates in
no way the bound for either possibility. That this lower bound seems to be satu-
rated has led to the speculation [43] that large-angle scattering takes place with a
minimal interaction, the cross section decreasing with the energy in the fastest pos-
sible way.

2.4.7. Summary

The previous paragraphs may be taken to indicate that, in spite of the great diver-
sity of models, there is no complete and satisfactory description of high-energy pp
scattering. Nevertheless several interesting general points emerge from the various
considerations. First, there is the possibility of a limiting or asymptotic angular dis-
tribution emerging at presently available energies, which may be related to the elec-
tromagnetic form factor of the proton. Next, multiple-scattering effects enter natu-
rally via several models and may be judged to be a possible universal feature of the
scattering outside of the main diffraction peak. Finally, the question of what actu-
ally may be learned about the structure of the proton in pp scattering experiments
is raised, the answer to this being very different depending upon the model favoured.

2.5. Nucleon resonance production in inelastic proton-proton scattering

2.5.1. Experimental summary

Systematic studies of the inelastic two-body process

$$p + p \to p + X$$
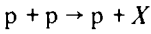
at high energies were first made by Chadwick et al. [44] and by Cocconi et al. [11, 45]. The experimental approach employed was that commonly called the "missing mass" method, in which forward-scattered protons were detected after magnetic analysis.

Taking (E_0, p_0) as the incident proton four-vector and (E, p) as that of the scattered proton, the missing mass M_X is given by

$$M_X^2 = (M + E_0 - E)^2 - (p_0 - p)^2 .$$ (6)

and hence

$$M_X^2 = M^2 + 2M(E_0 - E) + t .$$ (7)

For not too large angles and for high energies, eq. (7) may be simplified to give

$$\Delta p = \frac{M_X^2 - M^2}{2M} ,$$ (8)

where Δp is the difference in laboratory momentum at a fixed lab angle between elastically scattered protons and those inelastically scattered to produce a missing mass M_X.

The measured momentum spectra [11, 44, 45], in a range of $\Delta p \approx 2$ GeV/c, exhibited peaks superimposed on a continuous background. The peaks remained at a fixed Δp independent of energy and scattering angle, indicating the excitation of states of well-defined mass. In fact, the calculated values of the missing masses corresponded to those of three nucleon resonances found in pion-nucleon scattering phase-shift analyses [46] namely the isospin $I = \frac{3}{2}$ $\Delta(1236)$ and the isospin $I = \frac{1}{2}$ N(1520) and N(1688). In addition, there was the suggestion [45] of a peak at a mass of about 1.4 GeV excited at small momentum transfers, which was tentatively associated with an isospin $\frac{1}{2}$, p_{11} state found [47] in phase-shift analyses at a mass of 1.47 GeV.

In subsequent work by Bellettini et al [48], between 10 and 26.4 GeV/c, the strong excitation of a well-defined peak centred around a mass of 1.40 GeV was observed at very small momentum transfers ($|t| \lesssim 10^{-2}$ GeV^2) This result strengthened the belief that the peak corresponded to a nucleon resonance rather than to a kinematic effect [49].

Further work on single nucleon resonance production in two-body processes by the missing mass method may be listed as follows An extensive investigation of resonance production for $|t| \lesssim 1$ GeV^2 at incident momenta of 6, 10, 15, 20 and

30 GeV/c was made by Anderson et al. [50] who included the observation of the excitation of the isospin $\frac{1}{2}$ resonance N(2190). Data in this small t-range but at lower incident momenta, between 2.8 and 7.9 GeV/c, have been reported by Blair et al [51] and at very small $|t|$, less than 0.2 GeV^2, by Foley et al. [52]. The low energy (incident momenta between 3 and 7 GeV/c) and large momentum transfer region has been extensively studied by Ankenbrandt et al. [53], while Allaby et al. [54] have explored the large momentum transfer ($|t| \lesssim 6$ GeV^2) region at 19.2 GeV/c. The present experiment provides an extensive study at 24 GeV/c up to a $|t|$ value of 6 GeV^2.

2.5 2. General features of results

The angular distributions of the nucleon resonance reactions exhibit the general features, which have been outlined for elastic scattering in subsect. 2.1, of essentially all peripheral two-body hadronic reactions. The detailed form of the weakly energy-dependent forward peak ($\sim \exp [\ B|t|]$) depends, however, upon the resonance produced, the parameter B varying between about 4 GeV ^{2} for the N(1688) to about 18 GeV ^{2} for the N(1400) In this region the detailed dynamical features of the production process clearly play a role. For $|t| \geqslant 1$ GeV^2 the angular distributions of the production of the $\Delta(1236)$, N(1520) and N(1688) have been measured [53] in detail at energies up to 7 GeV, and they exhibit a flat t-dependence similar to elastic scattering at large momentum transfer

The most striking feature in the single resonance excitation is the difference in the energy dependence of the isospin $\frac{3}{2}$ state $\Delta(1236)$ and of the isospin $\frac{1}{2}$ states. It is found [50] that the production cross section for the isospin $\frac{1}{2}$ states is rather constant between 5 and 30 GeV/c, while that for the $\Delta(1236)$ decreases rapidly. This behaviour, an early and important result of these studies, indicates the dominance at high energies of processes in which minimal exchange of dynamical variables occur Production of a $\Delta(1236)$ necessitates an exchange process involving a unit of isospin, while the production of the N($I = \frac{1}{2}$) resonances is on an equal footing with elastic scattering in this respect requiring no change of isospin. These general ideas have been formulated [55] under the heading of "diffraction dissociation" processes in which the final states are, with regard to the important quantum numbers, identical to the initial states.

For this class of reaction an empirical selection rule has been proposed independently by Morrison [56] and by Gribov [57]. This rule constrains the parity change ΔP and the spin change ΔJ between the initial state and the final state particles (diffractively produced) to follow the relation $\Delta P = (-1)^{\Delta J}$. The bumps in the missing mass spectra at 1.52, 1.69 and 2.19 GeV indeed correspond to the mass values of known resonances whose spin-parity obey this rule. It has also been found to apply for meson-initiated reactions [52]

It should be noted that the present evidence for a great number of resonant states in the pion-nucleon system causes some difficulty in assigning unambiguously the established resonances to the bumps seen in the missing mass spectra. In fact

there is no experimental proof, at present, that each peak of the missing mass spectrum corresponds to the excitation of only one resonance, and not to a mixture of several of the many nucleon resonances known from phase-shift analyses.

2.5.3. Theoretical considerations

While the theoretical discussion of elastic pp scattering can invoke certain general features of collision theory, for example the use of the optical theorem to fix the imaginary part of the forward scattering amplitude, the discussion of the inelastic two-body processes $p + p \rightarrow p + X$ is, *a priori*, much more dependent on the details of specific models. For instance, it might be expected that changes of isospin, of spin and of parity in the final state resonance should have important dynamical consequences. However, as noted in subsect. 2.5.2, while observations indicate that the spin and parity cannot be ignored, it is the isospin character of the resonance which is the most important feature at high energies. Specifically the isospin $\frac{3}{2}$ $\Delta(1236)$ excitation has a strong energy dependence in its production, while the observed isospin $\frac{1}{2}$ states have essentially no energy dependence.

The general idea of diffraction dissociation [55] for the isospin $\frac{1}{2}$ resonances, although powerful in overall dynamical content, is quite vague in detail. Optical models based on this idea and on the older nuclear physics concept of "inelastic diffraction scattering" [58] have been elaborated by Feld [59] and by others [60], although without any very clear conclusion. The more general aspects of the diffractive excitation of the isospin $\frac{1}{2}$ states have been discussed by Chou and Yang [61]

In a related context some discussions [62], based on the Wu-Yang conjecture [29], have related the production of the isospin $\frac{1}{2}$ resonances to elastic scattering.

The basic difference in the energy dependences of the isospin $\frac{3}{2}$ and $\frac{1}{2}$ states is automatically accommodated in a conventional Regge-pole model, as evaluated, for example by Contogouris et al [63]. In this framework, the $I = \frac{1}{2}$ resonance production is the result of the Pomeranchuk trajectory exchange, while the $I = \frac{3}{2}$ $\Delta(1236)$ production is dominated by pion exchange. The energy dependence given by pion exchange is approximately s^{-2}, which is compatible with the data on the $\Delta(1236)$ production. A dominant pomeron exchange leads naturally to constant cross sections, as discussed by Frautschi et al [64], Contogouris et al. [63] and later by Margolis and Rottstein [65] for a trajectory with a slope of about 1 GeV $^{-2}$, as fitted by the data. However, complete conventional Regge-pole discussions involving more than a single trajectory contain all of the ambiguities and parametrisations of those describing elastic scattering.

The role of cuts in isospin $\frac{1}{2}$ resonance production has been discussed by Chiu and Finkelstein [36] and by Frautschi and Margolis [66] in treatments analogous to those used for elastic scattering. In general, Regge cuts, interpreted physically in terms of multiple scattering, would appear to be important at large momentum transfers and lead to rather universal angular distributions

Cross sections for nucleon resonance production have been calculated by Hendry and Trefil [67], employing the quark model and using the multiple scattering for-

malism of Glauber. In this approach the difference between the angular distributions
of the N(1400) and of the N(1688) production is explained by the difference in
their respective three-quark system wave functions, the former corresponding to a
radial excitation and the latter to an orbital excitation.

It may be concluded that while all of the theoretical formalisms applied to elas-
tic scattering may be applied to the resonance production processes with varying
degrees of success, there are two general ideas which remain the most important.
These are the general concepts of diffraction dissociation for isospin $\frac{1}{2}$ states and
the importance of multiple scattering effects at large momentum transfer.

3. The experimental technique

The experiment was performed at the CERN Proton Synchroton using a slowly
extracted proton beam incident on a liquid hydrogen target. The layout of the ex-
periment is shown in fig. 1. The forward-scattered protons were momentum anal-
ysed by a single-arm, magnetic spectrometer and detected by scintillation counter
hodoscopes.

The same apparatus was used to study other processes proton-neutron elastic
cross sections have been obtained from proton-deuteron scattering [68], the differ-
ential cross sections for the production of $d\pi^+$ and $d\rho^+$ from pp collisions have
been measured [69], a survey of particle production from pp collisions has been
reported [70]

3.1. Beam, target and monitoring

The extracted proton beam used at 24.0 GeV/c was the standard CERN facility
and had a spill length of about 350 msec and an intensity of about 10^{12} protons
every 2 sec. For the measurements at 10.0, 12.0 and 14.2 GeV/c, the extracted
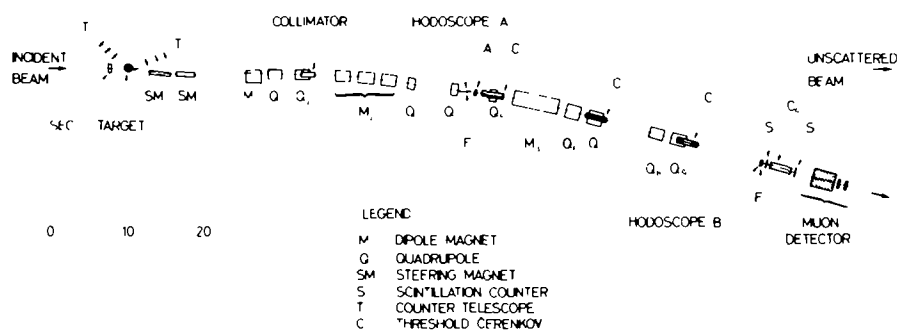proton beam was operated in a parasitic mode with a spill length of about 100 msec

Fig. 1. A plan view of the experimental equipment. The components are described in the text.

modulated by the RF structure of the accelerator The intensity of the beam in this mode was typically 10^{11} protons per pulse

The proton beam was focused onto the liquid hydrogen target where the spot size was approximately 4 mm diameter with a beam divergence of less than ± 0.5 mrad.

The liquid hydrogen target [71] was refrigerated by cold gaseous helium and was remotely controlled. The target cells were cylindrical and 4 cm in diameter with the axes aligned along the direction of the proton beam. Data were taken with cells of 10 and 20 cm length. The cells were composed of stainless steel and the end windows, through which the scattered particles passed, were each about 0.035 mm thick. The proton beam flux was monitored by a secondary emission chamber (shown as "SEC" in fig 1) placed 2.5 m ahead of the hydrogen target. Two triple-coincidence counter telescopes, T_1 and T_2, detecting secondary particles emitted from the target at 40° at at 140°, respectively, were used for relative monitoring of the beam intensity The secondary emission chamber and the counter telescopes were calibrated absolutely by measuring the ^{24}Na activity produced in thin aluminium foils placed in the beam ahead of the secondary emission chamber. An activation cross section for the aluminium foils of 8.6 + 0.5 mb [72] was assumed, independent of energy.

3.2. The magnetic spectrometer

The layout of the spectrometer is shown in fig. 1 The angle of the spectrometer with respect to the incident proton beam was fixed at 37 mrad. Particles produced in the target at 37 mrad were focused by the quadrupole doublet $Q_1 Q_2$ to an image of the target at F_1. The magnet M_2, composed of three standard 2 m bending magnets, produced a deflection of 120 mrad and a momentum dispersion at F_1 of 1 6 cm for $\Delta p/p = 1.0\%$. The quadrupole doublet $Q_6 Q_7$ produced a parallel beam which was foreseen to allow the use of a differential Čerenkov counter A 6 m long bending magnet M_3, producing a further bend of 120 mrad, was used to compensate the dispersive, momentum dependent change of inclination of the trajectories. In order to reduce the momentum-dependent displacement of the trajectories, the central plane of M_2 was imaged at the central plane of M_3 by means of the quadrupole triplet $Q_3 Q_4 Q_5$ acting as a field lens.

Thus, the optical transfer properties from the target to the exit of M_3 and further downstream were fairly achromatic, which is a desirable feature for clean particle identification and background rejection. In particular, the final focus at F_2, produced by the quadrupole doublet $Q_8 Q_9$, could be kept to a small size, given only by the chromatic aberration of the quadrupole lenses, the size of the source and multiple scattering in material along the spectrometer.

A ray diagram of the spectrometer optics is shown in fig. 2. A horizontal angular acceptance of ± 1.5 mrad and a vertical acceptance of ± 4.5 mrad were found to be safe in order to guarantee (by calculation) full transmission throughout the system
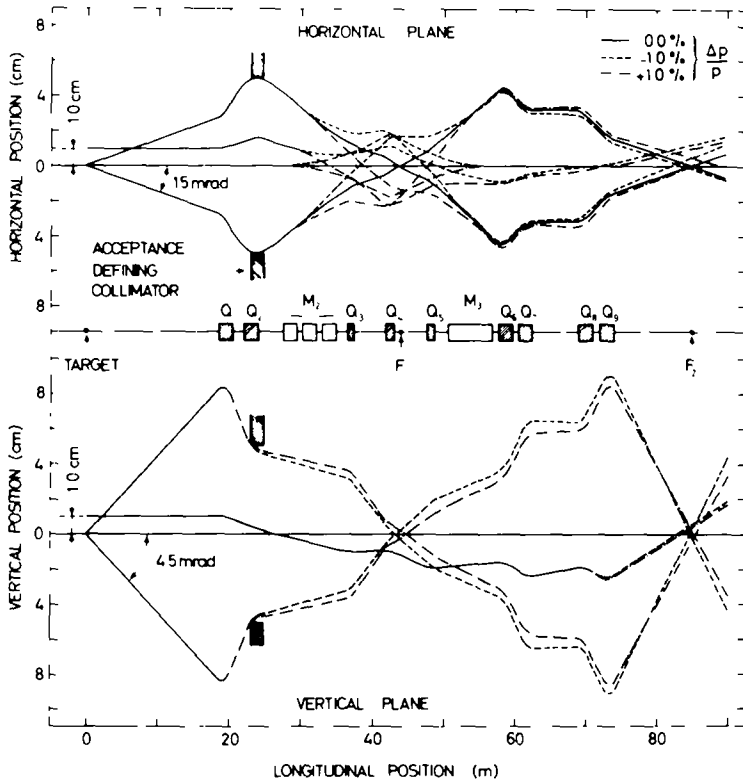
Fig. 2. Simplified ray-tracings of the spectrometer optics in the horizontal and vertical planes.

with a relative momentum interval of at least ± 1.5% of the central momentum and for displacements in the target plane of at least ± 1.5 cm. This acceptance could be defined conveniently by a cylindrical collimator of 10.0 cm diameter placed in the middle of Q_2, it was varied by using inserts of different diameters from 1.0 to 10.0 cm. The most frequently used collimator of 8.0 cm diameter thus defined (by calculation) a solid angle acceptance of 1 30 ± 10 [5] sterad. The ratios of the acceptance for different collimator sizes were repeatedly measured by observing the relative intensities of elastically scattered protons as well as for momenta at which the momentum distribution of scattered protons was flat. In view of the results of these measurements and of the shape of beam profiles at critical places (especially in the region Q_7 to Q_8) a ± 5% systematic uncertainty was assigned to the absolute value of the solid angle.

As mentioned above, the spectrometer axis was fixed at an angle of 37 mrad with respect to the incident beam direction. Scattering at angles other than 37 mrad could be measured by utilising the steering magnets SM_1, SM_2 and M_1. The septum magnets SM_1 and SM_2 were mounted on remotely-controlled carriages such that their

positions could be varied. M_1 was a 2m C-magnet fixed on the axis of the spectro-
meter. By varying the positions and currents of the magnets SM_1 and SM_2 and the
current of the magnet M_1, scattering angles in the range 12 to 152 mrad were se-
lected. This way of varying the horizontally accepted scattering angle as well as per-
forming the momentum analysis of the spectrometer in the same plane has the un-
desirable effect that, within the acceptance, the momentum is coupled to the hori-
zontal scattering angle θ by the relation

$$p(\theta \quad 37.0) = \text{constant} , \tag{9}$$

where 37 mrad is the fixed angle of the spectrometer with respect to the incident
beam direction. The implications of this effect on the procedure used in taking
data are discussed in subsect. 3 4.

The principal dispersive elements in the spectrometer, magnets M_2 and M_3, were
equipped with nuclear magnetic resonance probes. All dipole magnets contained
temperature stabilised Hall probes which were used for the on-line control of the
spectrometer. An absolute calibration of the spectrometer and steering magnets
was made, using the floating-wire technique, to an accuracy of $\Delta p/p = \pm 0.1\%$.

The length of the spectrometer from the target to the F_2 focus was 86 m. For
most of this distance the accepted particles were transmitted in a vacuum pipe in
order to keep absorption losses and multiple scattering to a minimum.

3.3. Particle detectors and electronics

The charged particles transmitted by the spectrometer were detected by two
scintillation counter hodoscopes A and B positioned at the foci F_1 and F_2, respec-
tively. Hodoscope A divided the momentum acceptance into nine channels of
$\pm 0.1\%$. For the data at small scattering angles there was adequate momentum reso-
lution using this hodoscope alone. However, at larger angles the momentum focus
at F_1 became smeared out due to the target length. Since the target is imaged at
the focus F_2, each of the five channels in the B hodoscope viewed a different region
of the target. Using the A hodoscope data in coincidence with each B hodoscope
channel it was possible to effectively reduce the target length and thus improve the
momentum resolution for the larger angle data (see subsect. 4.1 for further details).

The A hodoscope consisted of nine scintillation counters which provided the
nine contiguous momentum channels. Immediately downstream (see fig. 1), a larger
scintillation counter A'(4.0 cm wide by 3.0 cm high) accepted the full momentum
bite of the spectrometer. The B hodoscope was composed of three overlapping scin-
tillation counters which were used to provide five contiguous channels by means of
a suitable electronic logic. The counter S_1 (placed near F_2, with a scintillator size
of 4 0 cm wide by 3.0 cm high) and counter S_2 (5 m downstream from F_2) accepted
the full flux of particles transmitted by the spectrometer.

Fig. 3 shows a logic diagram illustrating how the pulses produced in the photo-
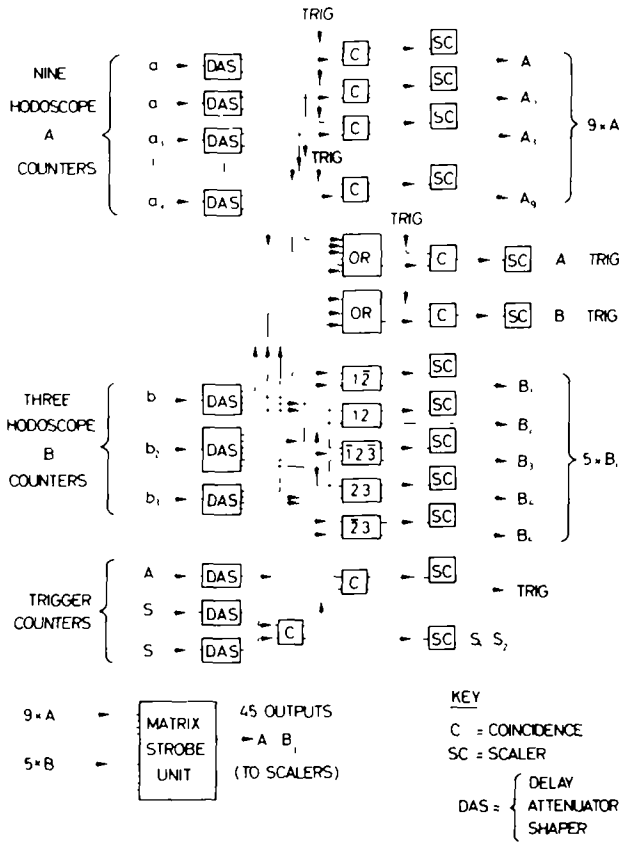multipliers were combined to form the various logical signals, which were recorded

Fig. 3. A logic diagram of the fast electronic circuitry.

on scalers. All combinations of the nine A_i channels and the five B_j channels were recorded on scalers in the form of a 45-element matrix with elements $A_i B_j$.

The spectrometer also contained four gas threshold Čerenkov counters (C_1 to C_4) and a muon detector (see fig. 1). Since for elastic proton-proton scattering and resonance production the pion and muon contaminations were found to be negligible, these detectors were not used. In fact, the Čerenkov counters were evacuated during these measurements to reduce multiple scattering and absorption losses. The Čerenkov counter system was used in particle production measurements [70].

During the data-taking of this experiment, raw cross sections $d^2\sigma/d\Omega\,dp$ from about 5×10^{-23} to 5×10^{-32} cm^2/sr GeV/c were recorded, that is, with counting rates varying from about 10^6 per sec. to 10^{-2} per sec. For a 10 cm hydrogen target and an 8 cm diameter collimator size, a cross section of 10^{-25} cm^2/sr · GeV/c at 24 GeV/c gave a counting rate of about 10^5 events per sec summed over the nine A channels. In order to measure the cross sections at small angles it was necessary to use the smaller-sized collimators to reduce electronic losses to below a few percent.
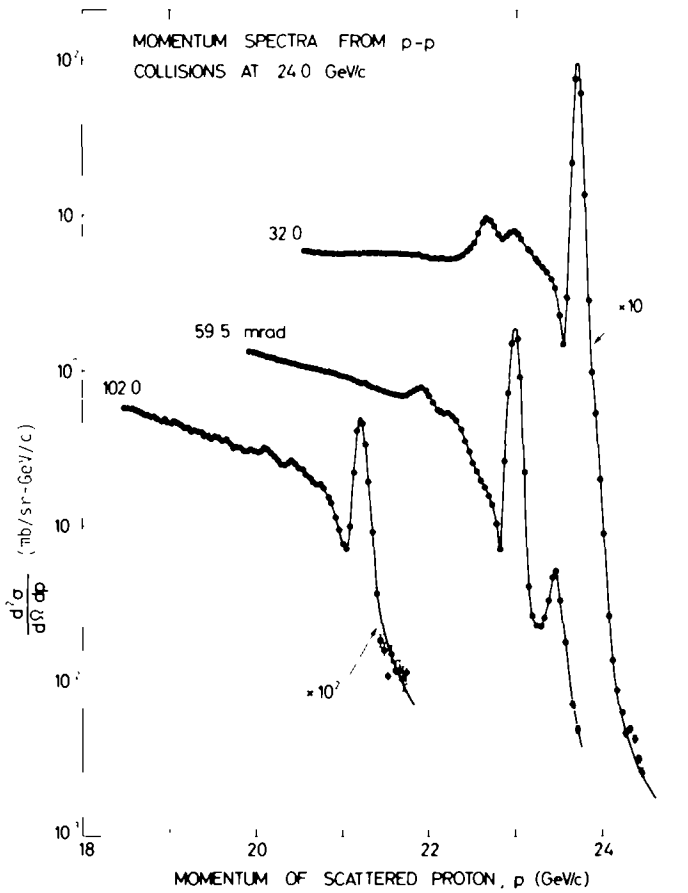
I ig. 4. Typical momentum spectra which illustrate the high resolution and good background rejection of the single-arm spectrometer technique.

The small aperture, long magnetic path-length, and two focal planes in the spectrometer provided an instrument with a high resolution in momentum and extremely good background rejection. Fig 4 contains some typical spectra which demonstrate the proton-proton elastic scattering and resonance production peaks over several orders of magnitude in count rate. The sharpness of the peaks and low levels of background, especially at momenta above that for elastic scattering, are clearly seen. The spectrum at 59.5 mrad also contains a peak at a momentum higher than that for elastic scattering which is due to macroscopic double scattering in the hydrogen target (see subsect 4.1).

3.4 Data collection

During the setting-up phase of the experiment a careful study was made of the performance of the spectrometer. All the magnetic elements were tuned experimentally with elastically scattered protons to obtain the optimum transmission at each momentum value. All current settings were found to be within a few percent of the calculated values. The momentum dispersion at F_1 was found to be 1.60 cm for $\Delta p/p = 1.0\%$, which is within 1% of the design value.

The spectrometer was controlled by a small on-line computer with 8 K of core memory. For a given incident momentum, proton scattering angle and secondary momentum, the computer calculated the required current settings for all the elements of the spectrometer and then set these values automatically. The relation between the momentum and current for each dipole and quadrupole magnet was expressed as a polynomial function. The currents in the quadrupoles and the voltages from the Hall probes in the bending magnets were monitored continuously while taking data. Small drifts in the settings were corrected automatically, for larger drifts, the intervention of the experimenter was required.

As mentioned above in subsect. 3.2, there was a coupling of the momentum dispersion of the spectrometer and the horizontal scattering angle as given by eq. (9). Thus the laboratory scattering angle θ varied over the 9 elements of the A hodoscope according to the relation (9), where the constant was determined by the θ, p values at the elastic scattering peak. During the measurement of a momentum spectrum, the momentum change from one setting to the next was, therefore, always correlated with a small change in the angular setting so that the two outer counters of the A hodoscope overlapped with the θ, p values of the previous setting. Thus, relation (9) ensured that at the overlapping counters the values of θ and p were the same for both settings.

Each data run lasted from 1 to 30 min, depending on the event rate. At the end of each run, the scaler data, trigger rates and beam monitoring information were recorded on punched cards and paper tape and, in parallel, transferred into the computer. The computer displayed the data on a graph plotter in the form of normalised momentum distributions and thus, over a period of several hours, built up a complete momentum spectrum containing both elastic and inelastic scattering. Data taking runs with the target empty were performed at regular intervals.

In order to plot the data as a momentum spectrum it was necessary to determine the product $\Delta\Omega \times \Delta p$ for each of the nine A counters (where $\Delta\Omega$ is the acceptance solid angle and Δp is the momentum bite of each counter). This was achieved by performing about five closely-spaced (overlapping) momentum scans over a reasonably flat region of the production spectrum (that is, at missing mass values greater than 2 GeV). These data were then fitted with a polynomial function using a least-squares fit computer program in order to obtain the relative quantity $\Delta\Omega \times \Delta p$ for each counter. The average value of these nine quantities was normalised to the value calculated for the middle of the nine A counters. The values obtained in this way

include geometric effects such as unequal scintillator sizes, counter efficiencies, etc. The values, which were determined experimentally every few days, were found to be reproducible throughout the whole experiment and to have a spread of a few percent around the calculated values.

4. Data analysis and results

4.1. Extraction of the elastic scattering cross sections

Angular distributions of proton-proton elastic scattering have been measured at 10.0, 12.0, 14.2 and 24.0 GeV/c over a range of lab scattering angles from 12 to 152 mrad. Some data have also been taken at 19.2 GeV/c to overlap with earlier measurements [1]. Preliminary values of these elastic data have already been reported [2].

The elastic cross sections were obtained by integrating the area under the elastic peak in the momentum spectra. Typical spectra are shown in figs. 5 and 6, which
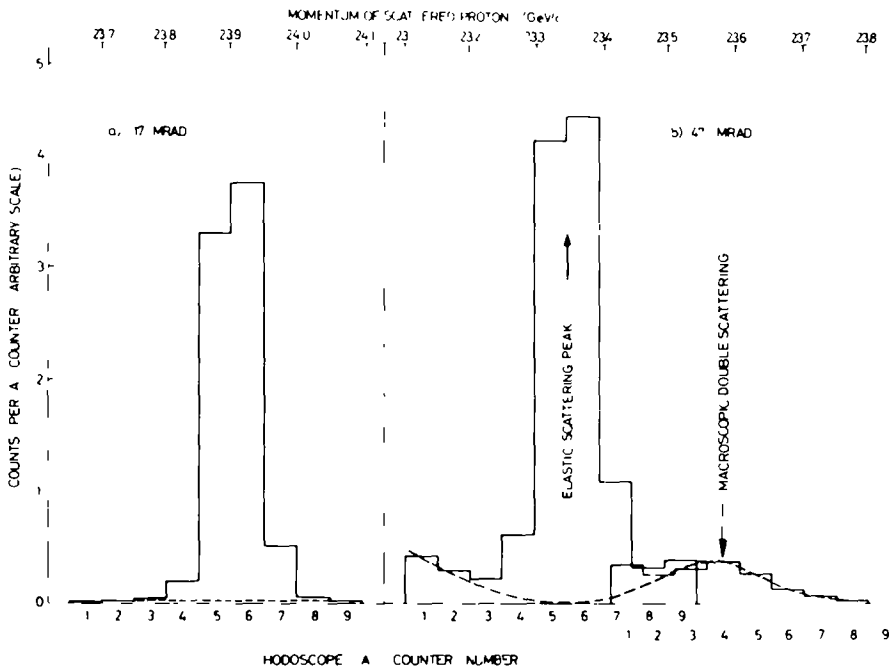
MOMENTUM OF SCAT FRED PROTON (GeV/c

| 237 | 238 | 239 | 24.0 | 24.1 | 23 | 23.2 | 23.3 | 23.4 | 23.5 | 23.6 | 23.7 | 23.8 |

COUNTS PER A COUNTER (ARBITRARY SCALE)

a) 17 MRAD

b) 47 MRAD

ELASTIC SCATTERING PEAK

MACROSCOPIC DOUBLE SCATTERING

HODOSCOPE A COUNTER NUMBER

Fig. 5. The momentum spectra from the A hodscope array showing the elastic proton-proton scattering peaks for (a) small and (b) intermediate scattering angles. The broken curves indicate the estimates of the background under the elastic scattering peaks.
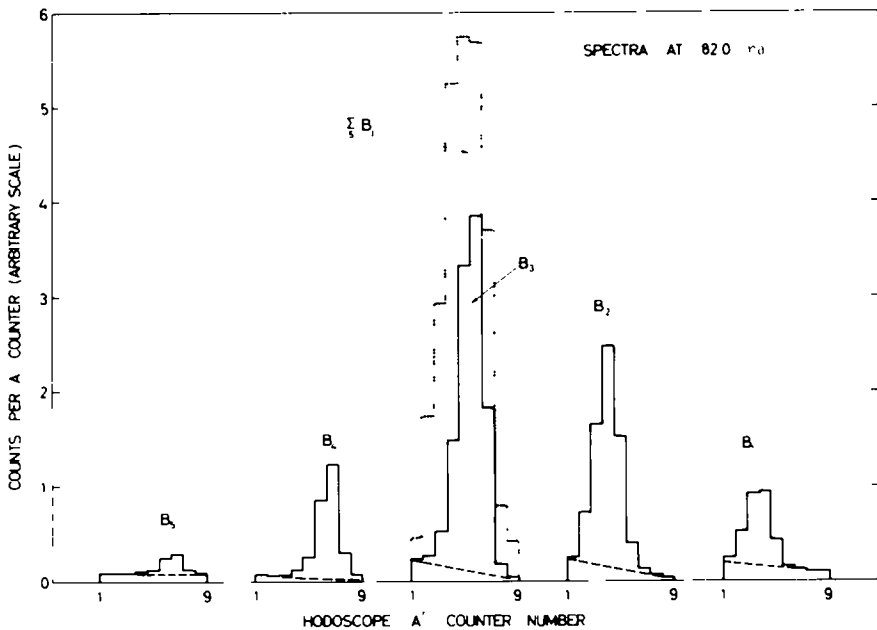
Fig. 6. The momentum spectra are shown for typical data at the larger scattering angles of this experiment. The spectra across the A hodoscope array are shown for those events in coincidence with each of the five counters of the B array. The broken curves indicate the estimates of the background under the elastic peaks. The dotted curve shows the deterioration in the momentum resolution when only the data in the A counter array is used.

are chosen to illustrate the characteristics of the background conditions at the small, intermediate and large angles of the present measurements.

For the data at small angles (fig. 5a), elastic scattering dominated and there was a negligible amount of background beneath the elastic peak in the momentum spectrum. At intermediate angles (fig. 5b) an estimate of the background under the elastic peak was made by linear extrapolation of the spectrum shape from the data on the low-momentum side of the peak. Because of the finite target length and the steep angular dependence of the cross section, protons which were scattered twice in the target gave an appreciable contribution to the momentum spectrum at intermediate angles as seen in fig. 5b (indicated as "macroscopic double scattering"). These protons have a known [68] momentum distribution extending above that of singly-scattered protons, and thus could be subtracted reliably. The accuracy of this subtraction was checked by comparing the data taken with 10 and 20 cm target lengths.

To extract the elastic peak events from the data at large angles, where there was a relatively larger background contribution and a broadening of momentum resolution due to the target length, a more refined treatment was required which used the

Table 1

Proton-proton elastic scattering cross sections at 10.0, 12.0, 14.2 and 24.0 GeV/c incident momenta

θ_{lab} (mrad)	10.0 GeV/c		12.0 GeV/c	
	$|t|$ (GeV^2)	$d\sigma/dt$ (cm^2/GeV^2)	$|t|$ (GeV^2)	$d\sigma/dt$ (cm^2/GeV^2)
27.0			0.104	3.57 E-26
32.0			0.146	2.59 E-26
37.0	0.135	1.96 E-26	0.195	1.57 E-26
42.0	0.173	1.74 E-26	0.251	9.89 E-27
47.0	0.217	1.29 E-26	0.313	5.95 E-27
52.0	0.264	8.09 E-27	0.382	3.41 E-27
57.0	0.317	4.60 E-27	0.458	1.88 E-27
62.0	0.374	3.34 E-27	0.540	9.89 E-28
67.0	0.435	1.84 E-27	0.628	4.99 E-28
72.0	0.501	1.31 E-27	0.722	2.47 E-28
77.0	0.571	6.71 E-28	0.822	1.20 E-28
82.0	0.645	4.13 E-28	0.928	5.95 E-29
87.0	0.723	2.32 E-28	1.04	3.03 E-29
92.0	0.804	1.40 E-28	1.16	1.83 E-29
97.0	0.890	8.52 E-29	1.28	1.20 E-29
102.0	0.980	4.47 E-29	1.40	8.96 E-30
107.0	1.07	3.08 E-29	1.54	8.14 E-30
112.0	1.17	1.86 E-29	1.67	7.08 E-30
117.0	1.27	1.76 E-29	1.81	5.92 E-30
122.0	1.37	1.32 E-29	1.96	5.06 E-30
127.0	1.48	1.09 E-29	2.11	4.05 E-30
132.0	1.59	9.42 E-30	2.26	3.41 E-30
137.0	1.70	8.33 E-30	2.42	2.73 E-30
142.0	1.81	7.18 E-30	2.57	2.17 E-30
147.0	1.93	6.29 E-30	2.74	1.68 E-30
152.0	2.05	5 07 E-30		

			24.0 GeV/c	
12.0			0.0828	3.05 E-26
13.5			0.105	2.62 E-26
14.5			0.121	2.45 E-26
15.1			0.131	2.16 E-26
17.0			0.166	1.59 E-26
19.5			0.218	1.12 E-26
22.0			0.277	6.08 E-27
24.5			0.343	3.78 E-27
27.0			0.416	1.74 E-27
29.5			0.496	1.04 E-27

Table 1, continued.

θ_{lab} (mrad)	14.2 GeV/c		24.0 GeV/c	
	$|t|$ (GeV^2)	$d\sigma/dt$ (cm^2/GeV^2)	$|t|$ (GeV^2)	$d\sigma/dt$ (cm^2/GeV^2)
32.0			0.582	4.95 1-28
34.5			0.675	2.53 1-28
37.0	0.273	6.51 1-27	0.775	9.42 F-29
39.5			0.881	3.86 L-29
42.0	0.351	3.27 E-27	0.994	1.45 1-29
44.5			1.11	6.37 1-30
47.0	0.438	1.59 E-27	1.24	3.37 1-30
49.5			1.37	2.47 L-30
52.0	0.535	7.22 F-28	1.51	2.16 1-30
54.5			1.65	1.96 1-30
57.0	0.640	2.93 E-28	1.80	1.61 F-30
59.5			1.95	1.29 F-30
62.0	0.754	1.20 1-28	2.11	9.67 1-31
64.5			2.28	7.64 F-31
67.0	0.876	4.36 1-29	2.45	5.42 1-31
72.0	1.01	1.96 1-29	2.80	2.79 L-31
77.0	1.15	1.06 1-29	3.18	1.26 E-31
82.0	1.29	6.93 1-30	3.57	6.80 1-32
87.0	1.45	6.07 1-30	3.98	3.11 1-32
92.0	1.61	5.02 1-30	4.40	1.49 1-32
97.0	1.77	4.23 F-30	4.84	7.73 E-33
102.0	1.95	3.39 F-30	5.30	4.72 F-33
107.0	2.13	2.45 1-30	5.76	2.61 F-33
112.0	2.31	1.91 1-30	6.24	1.61 E-33
117.0	2.51	1.34 F-30	6.72	8.49 L-34
122.0	2.70	1.00 E-30		
127.0	2.90	6.92 1-31		
132.0	3.11	4.89 1-31		
137.0	3.32	3.44 E-31		
142.0	3.54	2.41 L-31		

The lab angles for the forward-scattered protons are shown together with the corresponding value of the four-momentum transfer squared $|t|$. The statistical errors in the data are small (typically ~ 1%), however there is an estimated random error in the data points of ± 6% at 24.0 GeV/c and ± 8% at the other momenta due to the lack of reproducibility at each setting. There is an overall normalisation uncertainty in the data which is estimated to be ± 10% at 24.0 GeV/c and ± 15% at the other momenta.

information from the B hodoscope counters. As mentioned in subsect. 3.3, the B counters effectively cut up the target into several smaller regions and thus an improved momentum resolution was obtained. The momentum spectrum in the A_i counters was plotted for each of the five B_j counters and the background contribution under each elastic scattering peak, which varied across the hodoscope arrays, was estimated as indicated by the broken curves in fig. 6. The elastic peak cross sections were then calculated from the sum of the elastic peaks in the five B counters The poorer momentum resolution obtainable with the A counters alone is indicated by the dotted curve in fig. 6. The information provided by the coincidences between the two arrays of counters allowed a momentum resolution of $\pm 0.2\%$ to be maintained at all angles

Empty-target subtractions varied from 1 to 8%, depending upon the scattering angle. The amount of material through which the protons passed was minimised by employing vacuum pipes wherever possible in the spectrometer. Nevertheless there still remained about $8 \, \text{g} \cdot \text{cm}^{-2}$ of windows, scintillators and residual air, leading to a correction for proton absorption which was calculated using the nuclear inelastic and elastic cross sections of Bellettini et al [73]. The correction was about 10% at all the energies of the experiment Corrections for dead-times and accidentals were in general a few percent, however, for measurements at the smallest angles, corrections of up to 10% were applied. Pion contamination was negligible, even for the data at large angles. Target boiling was calculated to be negligible during these measurements.

The final elastic cross section values are given in table 1. The statistical errors of the measurements were negligible compared with the systematic uncertainty. After considering the spread in values of some repeatedly measured points, errors were assigned to the data of $\pm 6\%$ at 24.0 GeV/c and $\pm 8\%$ at the other momenta These errors are believed to arise from the uncertainty and irreproducibility in the incident beam direction. In addition, at 24.0 GeV/c there is an overall scale error of $\pm 10\%$, mainly resulting from the $\pm 7\%$ uncertainty in the ^{24}Na activation cross section and $\pm 5\%$ uncertainty in the solid angle of the spectrometer. At 10.0, 12 0 and 14.2 GeV/c the scale error is estimated to be $\pm 15\%$ due to the smaller number of repeated measurements at these energies and to the poorer beam conditions during these runs.

4.2. Analysis of the nucleon resonance production

Nucleon resonance production has been measured over the range of four-momentum transfer squared, $|t|$, from 0.1 to 6 4 GeV^2 for an incident 24.0 GeV/c proton beam momentum. Fig. 7 shows all the momentum spectra collected, where the data have been converted into the differential cross section $d^2\sigma/dt \, dM$. Preliminary results have been published previously [3]. Some typical spectra are shown in more detail in fig. 8 For each spectrum the value of $|t|$ changes by a small amount over the explored missing mass range ($M < 2.6$ GeV) because the spectra were measured at angles and momenta given by eq. (9).
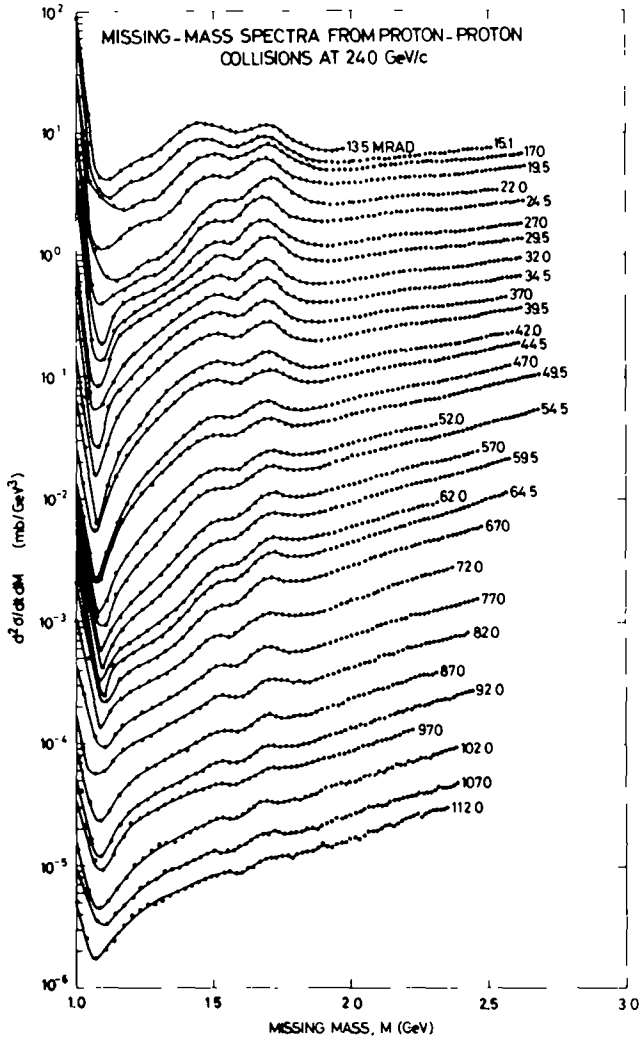
Fig. 7. A logarithmic scale plot of all the missing mass spectra taken at 24.0 GeV/c. The lab angle (mrad) of the forward elastically scattered proton is given with each curve. The elastic scattering peaks are not shown in the figure.

The measured spectra contain two distinct peaks at missing mass values near 1.52 and 1.69 GeV. For $|t|$ values less than about 1.7 GeV^2 there is a wide bump present around $M = 2.2$ GeV. At $|t|$ values less than 0.3 GeV^2 there is evidence for a shoulder around $M = 1.4$ GeV on the low-mass side of the peak at $M = 1.52$ GeV. Following the usual interpretation, as discussed in subsect. 2.5, the three prominent
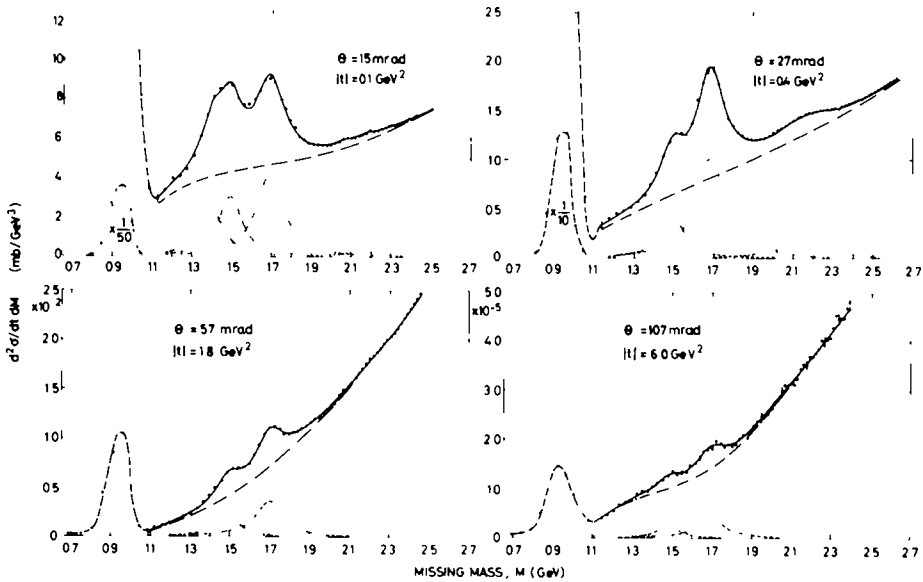
Fig. 8. Typical momentum spectra of forward-scattered protons from proton-proton collisions at 24.0 GeV/c. The quantity θ denotes the proton scattering angle and t is the four-momentum transfer squared value corresponding to elastic scattering. The fitted curves to the measured points are shown together with the individual resonance and background contributions.

bumps are assumed to result from the excitation of the N(1520), N(1688) and N(2190) resonances, and the shoulder around $M = 1.4$ GeV is considered to correspond to the excitation of an N(1400) resonance.

The resonance production cross sections have been extracted from each missing mass spectrum by fitting the spectrum with a sum of resonant terms (having Breit-Wigner shapes) and a polynomial term representing the continuum, of the form

$$\left(\frac{d^2\sigma}{dt\,dM}\right) = \sum_k c_k M^k + \sum_i \frac{a_i}{2\pi}\left\{\frac{\Gamma_i}{(M-M_i)^2+(\frac{1}{2}\Gamma_i)^2}\right\}, \tag{10}$$

where M_i and Γ_i are the mass and width of the ith resonance, respectively, c_k is a coefficient and a_i represents the differential cross section for resonance production, i.e. the area of the Breit-Wigner curve. A computer program was used to obtain the least-squares solution for the polynomial coefficients, the cross sections and some of the masses and widths of the resonances. In the typical spectra, shown in fig. 8, the solid curves are the fitted forms of eq. (10) and the broken curves indicate the resonance and polynomial contributions.

The widths of the two peaks at $M \simeq 1.52$ and $M \simeq 1.69$ GeV were determined by fitting some high-statistics spectra at intermediate momentum transfer values where there was little N(1400) contribution. The two widths after unfolding the

experimental resolution were 118 ± 20 MeV and 152 ± 15 MeV, respectively. These two values have been used as fixed parameters in the final fitting procedure. For the mass and width of the N(1400) the values obtained from other experiments [48, 50, 51, 74] have been taken 1.41 GeV and 150 MeV, respectively. The width of the N(2190) could not be extracted from the data and was taken as 250 MeV, which is typical of previous measurements. Varying the N(2190) width from 200 to 300 MeV changed the resonance cross section by about a factor of 2, essentially independent of momentum transfer. This variation has been taken into account in assigning the errors to these cross sections. Another check performed was to use Gaussians for the shape of the resonance peaks. It was found that resonance cross sections about a factor 2 smaller than for the Breit-Wigner forms resulted from such fits.

In the fitting procedure, the cross sections, the coefficients of the polynomial and the masses of the three peaks corresponding to the N(1520), N(1688) and N(2190) were left as free parameters. The values of the masses of the three peaks deduced from the best fits to all the spectra were 1500 ± 10 MeV, 1694 ± 8 MeV and 2160 ± 50 MeV, respectively. The cross sections obtained from the best fit were found to be insensitive to the order of the background polynomial, which was varied between 4 and 6. Polynomials of order 4 were finally adopted. The χ^2 values corresponding to the best fits were always reasonable.

The values of the mass and width of the peaks determined by means of the fitting procedure are given in table 2, together with the results obtained with incident protons of lower energy [50, 53] and from reactions initiated by negative pions [74] and electrons [75]. The figures reported in a compilation [46] of phase-shift analyses are also shown for comparison. The satisfactory agreement among the different determinations of masses and widths shown in table 2 is the basis of the conventional interpretation that the peaks observed in the missing mass spectra are principally due to the excitation of these particular resonances.

The problem of obtaining the N(1400) cross sections is indicated in fig. 9. At moderate momentum transfer, for example at $|t| = 0.37$ GeV^2, the shape of the missing mass spectrum around $M = 1.4$ GeV is well-reproduced by the tail of the Breit-Wigner function which fits the N(1520) peak. At smaller momentum transfers the shape of the spectrum is very different and an adequate fit cannot be obtained without introducing a resonance with a mass of about 1.4 GeV. At larger momentum transfers, the shape of the spectrum is also different and can be well represented by including the N(1400) in the fit. However, it is also possible, for $|t| > 0.5$ GeV^2, to produce a reasonable fit without the N(1400) by allowing the background to have a discontinuous change between moderate and high $|t|$ regions. It has been assumed that such a discontinuity is unlikely, and the cross sections and errors for N(1400) production have been evaluated from fits to the mass-spectra even beyond $|t| = 0.5$ GeV^2.

In addition to the resonances already mentioned, there was also a small enhancement close to the tail of the elastic peak. This was identified as the $I = \frac{3}{2}$, $\Delta(1236)$

Table 2
The mass M and width Γ in MeV for the N(1520), N(1688) and N(2190) resonances as reported by several groups

Experiment			N(1520)		N(1688)		N(2190)	
Initial state	Momentum (GeV/c)	Ref.	M	Γ	M	Γ	M	Γ
pp	3– 7	[53]	1508 ± 2	92 ± 3	1683 ± 3	110 ± 4		
pp	6–30	[50]	1501 ± 6	140 ± 43	1690 ± 5	133 ± 26		
pp	24	this expt.	1500 ± 10	118 ± 20	1694 ± 8	152 ± 15	2160 ± 50	
π⁻p	8,16	[74]	1503 ± 6	105 ± 9	1691 ± 4	119 ± 9	2180 ± 25	265 ± 70
ep	7–17	[75]	1508 ± 5	80 ± 20	1705 ± 15	85 ± 25		
	phase-shift analyses	[46]	1521 ± 9	121 ± 12	1688 ± 4	125 ± 21	2176 ± 97	306 ± 11
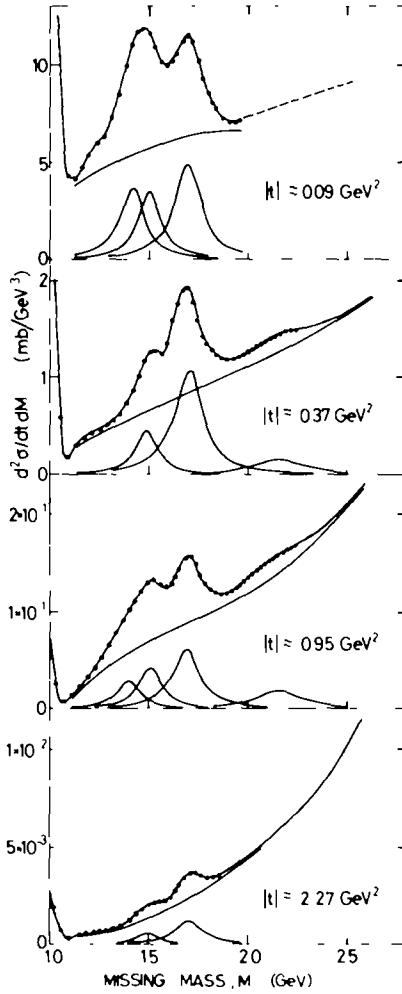
Fig. 9. Typical momentum spectra illustrating the difficulty of extracting a cross section for the N(1400) resonance.

resonace which is known [48, 50, 51] to be only weakly excited in pp collisions at high energies. The production cross section of this resonance could not be extracted by the above fitting procedure due to the difficulty of fitting the continuum near to its kinematic limit, which is also close to the tail of the elastic peak. Thus qualitative values for the cross sections were estimated using the graphical procedure illustrated in fig. 10.

The final values of the resonance production cross sections are given in table 3. These data are affected by an overall scale error of ± 15%, mainly due to the uncer-
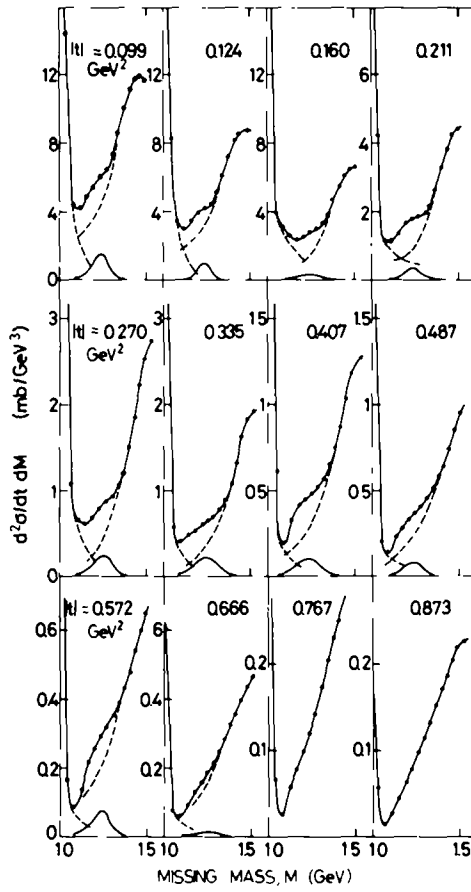
Fig. 10. Typical momentum spectra at $|t|$ values < 0.9 GeV^2 showing the evidence for the $\Delta(1236)$ resonance. The tail from the elastic scattering peak and the non-negligible background contribution in the region of the $\Delta(1236)$ make it difficult to estimate the cross section for this resonance production.

tainty in the beam calibration, as discussed in subsect. 4.1, and to the background subtraction procedure.

Values of the polynomial background cross sections resulting from the fitting of the spectra by eq. (10) are listed in table 4. The values of $d\sigma/dt$ for the non-resonant background have been calculated at each value of missing mass (M_i GeV) and are normalised to an effective width of 1.00 GeV in missing mass according to the relation

$$\left(\frac{d\sigma}{dt}\right)_{M=M_i} = \frac{1.00\ (\text{GeV})}{\Delta M} \int_{M_i - \frac{1}{2}\Delta M}^{M_i + \frac{1}{2}\Delta M} \left(\frac{d^2\sigma}{dt\ dM}\right)_{\text{background}} dM\ , \tag{11}$$

Table 3

Resonance production cross sections in proton-proton collisions at 24.0 GeV/c

θ_{lab} (mrad)	$|t|$ (GeV^2)	$d\sigma/dt$ (cm^2/GeV^2)
		$\Delta(1236)$
13.5	0.099	$(1.7 \; {}^{+1.7}_{-0.8} \;)$ I-28
15.1	0.124	$(1.1 \; {}^{+1.1}_{-0.6} \;)$ Γ-28
17.0	0.160	$(4.4 \; {}^{+4.4}_{-2.2} \;)$ I-29
19.5	0.211	$(3.3 \; {}^{+3.3}_{-1.7} \;)$ I-29
22.0	0.270	$(2.2 \; {}^{+2.2}_{-1.1} \;)$ Γ-29
24.5	0.335	$(2.2 \; {}^{+2.2}_{-1.1} \;)$ I-29
27.0	0.407	$(1.1 \; {}^{+1.1}_{0.6} \;)$ I-29
29.5	0.487	$(1.1 \; {}^{+1.1}_{-0.6} \;)$ Γ-29
32.0	0.572	$(8.0 \; \pm 8.0 \;)$ E-30
34.5	0.666	$(2.2 \; \pm 2.2 \;)$ Γ-30
37.0	0.767	$(0.0 \; \pm 1.1 \;)$ I-30
39.5	0.873	$(0.0 \; \pm 1.1 \;)$ I-30
		$N(1400)$
13.5	0.094	(1.08 ± 0.22) I-27
15.1	0.119	$(6.6 \; \pm 1.3 \;)$ L-28
17.0	0.155	$(3.1 \; \pm 0.7 \;)$ I-28
19.5	0.206	$(0.0 \; \pm 2.2 \;)$ I-29
22.0	0.264	$(1.2 \; \pm 0.8 \;)$ Γ-29
24.5	0.328	$(0.0 \; \pm 6.0 \;)$ I-30
27.0	0.401	$(0.0 \; \pm 2.2 \;)$ E-30
29.5	0.480	$(0.0 \; \pm 2.2 \;)$ E-30
32.0	0.565	$(9.0 \; \pm 8.0 \;)$ I-31
34.5[a]	0.659	$(1.7 \; \pm 0.4 \;)$ Γ-29
37.0[a]	0.760	$(1.5 \; \pm 0.4 \;)$ I-29
39.5[a]	0.867	$(1.0 \; \pm 0.3 \;)$ I-29
42.0[a]	0.978	$(8.0 \; \pm 2.0 \;)$ Γ-30
44.5[a]	1.10	$(5.0 \; \pm 1.3 \;)$ I-30
47.0[a]	1.22	$(1.8 \; \pm 0.5 \;)$ Γ-30
49.5[a]	1.36	$(1.2 \; \pm 0.3 \;)$ I-30
52.0[a]	1.49	$(4.4 \; \pm 1.1 \;)$ I-31
		$N(1520)$
13.5	0.091	$(8.2 \; {}^{+1.1}_{-3.3} \;)$ I-28
15.1	0.116	$(6.4 \; {}^{+1.1}_{3.3} \;)$ I-28

Table 3, continued (1)

θ_{lab} (mrad)	$|t|$ (GeV^2)	$d\sigma/dt$ (cm^2/GeV^2)
	N(1520) continued	
17.0	0.151	$(7.0 \begin{smallmatrix}+1.1\\-2.8\end{smallmatrix})$ 1-28
19.5	0.202	(4.4 ± 1.1) 1-28
22.0	0.259	(2.89 ± 0.44) 1-28
24.5	0.323	(1.89 ± 0.33) Γ-28
27.0	0.396	(1.07 ± 0.16) 1-28
29.5	0.475	(7.4 ± 1.1) 1-29
32.0	0.560	(4.4 ± 0.7) 1-29
34.5	0.654	(3.6 ± 0.6) 1-29
37.0	0.754	(2.44 - 0.44) 1-29
39.5	0.862	(1.55 ± 0.22) 1-29
42.0	0.973	(1.03 · 0.16) 1-29
44.5	1.09	(6.8 ± 1.0) Γ-30
47.0	1.22	(3.3 ± 0.6) 1-30
49.5	1.35	(2.11 ± 0.33) 1-30
52.0	1.49	(1.33 · 0.22) 1-30
54.5	1.64	(8.9 ± 1.3) Γ-31
57.0	1.79	(4.7 ± 0.7) 1-31
59.5	1.94	(2.89 ± 0.44) 1-31
62.0	2.10	(2.11 ± 0.33) Γ-31
64.5	2.27	(1.33 ± 0.22) 1-31
67.0	2.44	(8.9 ± 1.3) 1-32
72.0	2.80	(5.4 ± 0.9) 1-32
77.0	3.19	(2.89 ± 0.44) 1-32
82.0	3.60	(1.78 ± 0.33) 1-32
87.0	4.01	(7.4 ± 1.4) 1-33
92.0	4.45	(2.9 ± 0.6) Γ-33
97.0	4.90	(1.44 ± 0.33) 1-33
102.0	5.37	(7.4 ± 1.4) 1-34
107.0	5.86	(5.7 ± 1.7) 1-34
112.0	6.35	(2.1 ± 0.7) Γ-34
	N(1688)	
13.5	0.087	(1.48 + 0.17) 1-27
15.1	0.111	(1.21 ± 0.11) L-27
17.0	0.145	(1.21 ± 0.11) Γ-27
19.5	0.196	(9.3 · 0.9) L.28
22.0	0.252	(7.0 ± 0.7) 1-28
24.5	0.317	(4.77 ± 0.44) 1-28
27.0	0.388	(3.09 ± 0.33) 1-28
29.5	0.467	(2.11 ± 0.22) 1-28
32.0	0.552	(1.19 ± 0.11) Γ-28
34.5	0.646	(8.6 ± 0.9) 1-29
37.0	0.747	(4.91 ± 0.44) Γ-29
39.5	0.853	(3.33 ± 0.33) 1-29
42.0	0.965	(1.74 ± 0.18) 1-29

Table 3, continued (2).

θ_{lab} (mrad)	$|t|$ (GeV^2)	$d\sigma/dt$ (cm^2/GeV^2)
		N(1688) continued
44.5	1.09	(1.14 ± 0.11) I-29
47.0	1.21	$(5.8 \pm 0.6$) I-30
49.5	1.35	(3.81 ± 0.33) I-30
52.0	1.48	(2.32 ± 0.22) I-30
54.5	1.63	(1.47 ± 0.11) I-30
57.0	1.78	(1.04 ± 0.10) I-30
59.5	1.94	$(7.8 \pm 0.8$) I-31
62.0	2.10	$(5.9 \pm 0.6$) I-31
64.5	2.27	(3.44 ± 0.33) I-31
67.0	2.44	(2.55 ± 0.22) I-31
72.0	2.80	(1.28 ± 0.11) I-31
77.0	3.19	$(5.8 \pm 0.6$) I-32
82.0	3.61	$(2.8 \pm 0.6$) I-32
87.0	4.03	(1.22 ± 0.22) I-32
92.0	4.47	$(5.2 \pm 1.1$) I-33
97.0	4.92	$(3.1 \pm 0.6$) I-33
102.0	5.40	(1.22 ± 0.22) I-33
107.0	5.89	(1.22 ± 0.33) I-33
112.0	6.39	$(4.1 \pm 1.1$) I-34
		N(2190)
15.1	0.097	(1.04 ± 0.29) I-28
17.0	0.130	(1.02 ± 0.32) I-28
19.5	0.178	$(8.3 \pm 2.8$) I-29
22.0	0.232	$(7.5 \pm 2.2$) I-29
24.5	0.295	$(7.2 \pm 2.1$) I-29
27.0	0.365	$(6.3 \pm 1.8$) I-29
29.5	0.443	$(5.5 \pm 1.8$) I-29
32.0	0.527	$(4.0 \pm 1.2$) I-29
34.5	0.621	$(2.6 \pm 0.8$) I-29
37.0	0.721	$(1.9 \pm 0.6$) I-29
39.5	0.829	(1.28 ± 0.44) I-29
42.0	0.941	$(7.4 \pm 2.3$) I-30
44.5	1.06	$(4.8 \pm 2.2$) I-30
47.0	1.19	$(2.8 \pm 1.3$) I-30
49.5	1.33	$(1.5 \pm 0.7$) I-30
52.0	1.46	$(5.6 \pm 2.8$) I-31

The lab angles for the forward-scattered protons are shown together with the value of the four-momentum transfer squared $|t|$ for each resonance. In addition to the random errors quoted in the table, there is an overall normalisation uncertainty which is estimated to be $\pm 15\%$, except for the N(2190) where the error is $\pm 30\%$ due to the uncertainty in the width.

[a] These data have an additional uncertainty due to the possible ambiguity in the fitting procedure (see subsect. 4.2)

Table 4

Non-resonance background production cross sections in proton-proton collisions at 24.0 GeV/c

Missing mass (GeV)	1.5		2.0		2.5	
θ_{lab} mrad	$\lvert t\rvert$ GeV²	dσ/dt (cm²/GeV²)	$\lvert t\rvert$ GeV²	dσ/dt (cm²/GeV²)	$\lvert t\rvert$ GeV²	dσ/dt (cm²/GeV²)
13.5	0.092	6.33 I -27	0.079	7.22 I -27		
15.1	0.117	4.86 I -27	0.102	5.87 I -27	0.089	8.10 I -27
17.0	0.152	3.20 I -27	0.135	5.08 I -27	0.120	6.83 I -27
19.5	0.203	2.62 I -27	0.184	3.93 I -27	0.165	5.28 I -27
22.0	0.260	1.34 I -27	0.239	2.67 I -27	0.218	3.68 I -27
24.5	0.324	1.04 I -27	0.302	1.96 I -27	0.279	2.79 I -27
27.0	0.396	7.21 I -28	0.373	1.23 I -27	0.348	1.81 I -27
29.5	0.476	5.81 I -28	0.452	8.74 I -28	0.426	1.37 I -27
32.0	0.561	4.39 I -28	0.536	5.81 I -28	0.509	9.34 I -28
34.5	0.655	2.68 I -28	0.630	4.09 I -28	0.602	6.64 I -28
37.0	0.756	1.71 I -28	0.730	2.56 I -28	0.703	4.57 I -28
39.5	0.862	1.40 I -28	0.838	2.13 I -28	0.810	3.63 I -28
42.0	0.973	7.68 I -29	0.950	1.31 I -28	0.923	2.29 I -28
44.5	1.09	5.78 I -29	1.07	1.02 I -28	1.05	1.82 I -28
47.0	1.22	3.05 I -29	1.19	6.57 I -29	1.17	1.24 I -28
49.5	1.35	2.37 I -29	1.33	5.00 I -29	1.31	9.23 I -29
52.0	1.49	1.15 I -29	1.47	3.01 I -29	1.45	6.50 I -29
54.5	1.64	9.04 I -30	1.62	2.37 I -29	1.61	4.66 I -29
57.0	1.79	4.69 I -30	1.78	1 44 I -29	1.76	2.80 I -29
59.5	1.94	3.24 I -30	1.93	1.01 I -29	1.93	2.14 I -29
62.0	2.10	1.70 I -30	2.10	6 53 I -30	2.09	1.50 I -29
64.5	2.27	1.46 I -30	2.27	4.85 I -30	2.27	1.12 I -29
67.0	2.44	9.14 I -31	2.44	3.12 I -30	2.45	6.80 I -30
72.0	2.80	5.31 I -31	2.81	1.62 I -30	2.83	3.20 I -30
77.0	3.18	3.08 I -31	3.20	8.36 I -31	3.24	1.76 I -30
82.0	3.60	1.78 I -31	3.63	4.66 I -31	3.68	1.00 I -30
87.0	4.01	9.89 I -32	4.06	2.56 I -31	4.12	6.00 I -31
92.0	4.45	6.08 I -32	4.51	1.47 I -31	4.60	3.37 I -31
97.0	4.90	4.43 I -32	4.98	9.91 I -32	5.08	2.00 I -31
102.0	5.37	2.23 I -32	5.46	5 46 I -32	5.61	1.23 I -31
107.0	5.85	1.15 I -32	5.97	2.89 I -32	6.14	5.68 I -32
112.0	6.35	8.06 I -33	6.48	1.86 I -32	6.69	3.20 I -32

The values of dσ/dt have been obtained by integration over a missing mass interval of 1.0 GeV using eqs (10) and (11), as explained in the text. The lab angle corresponds to the elastically scattered protons for each spectra. There is an estimated normalisation uncertainty in the data of ± 20%.

where ΔM is a small interval of missing mass. From considerations of the fitting procedure and the smoothness of the background at different angles, an estimated uncertainty of ± 20% is assigned to these data in the table.

5. Discussion of results

5.1. Elastic proton-proton scattering

5.1.1. The structure in the angular distribution

The cross sections for elastic proton-proton scattering given in table 1 are shown in fig. 11 together with other published data [1, 18, 20, 53, 76]. The shoulder-like
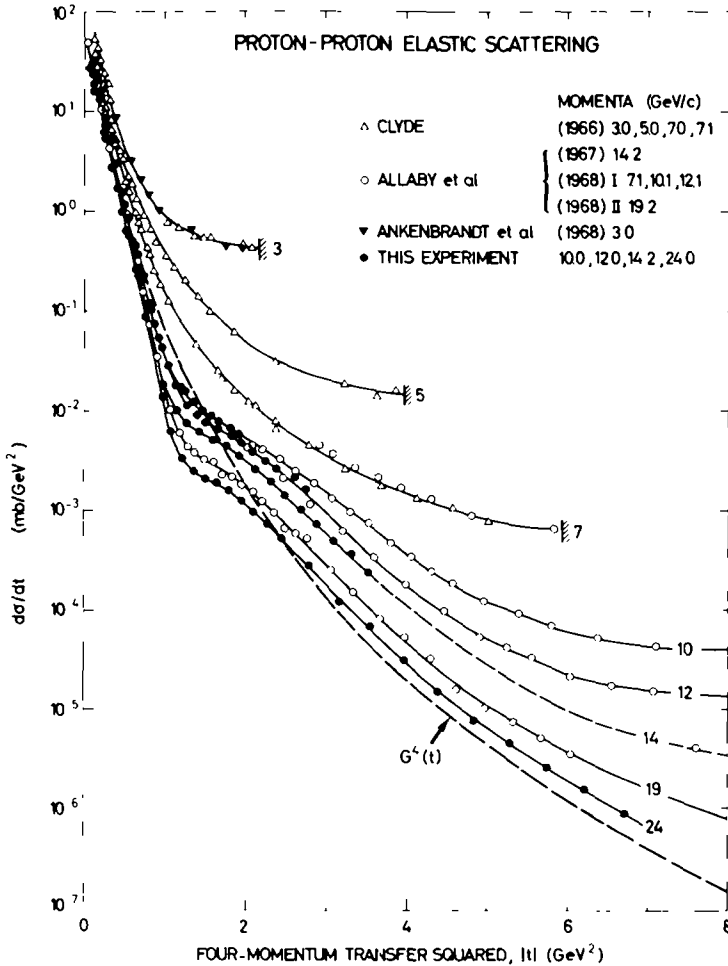
Fig. 11. Angular distributions for proton-proton elastic scattering. The data at the same incident momentum have been joined by a smooth curve. The symbol at the end of the curves corresponding to the low-energy data indicates 90° c.m.. The curve labelled $G^4(t)$ shows the variation of the fourth power of the dipole form of the electromagnetic form factor of the proton. The data included in this figure have been taken from refs [1, 18, 20, 53, 76] and this experiment.
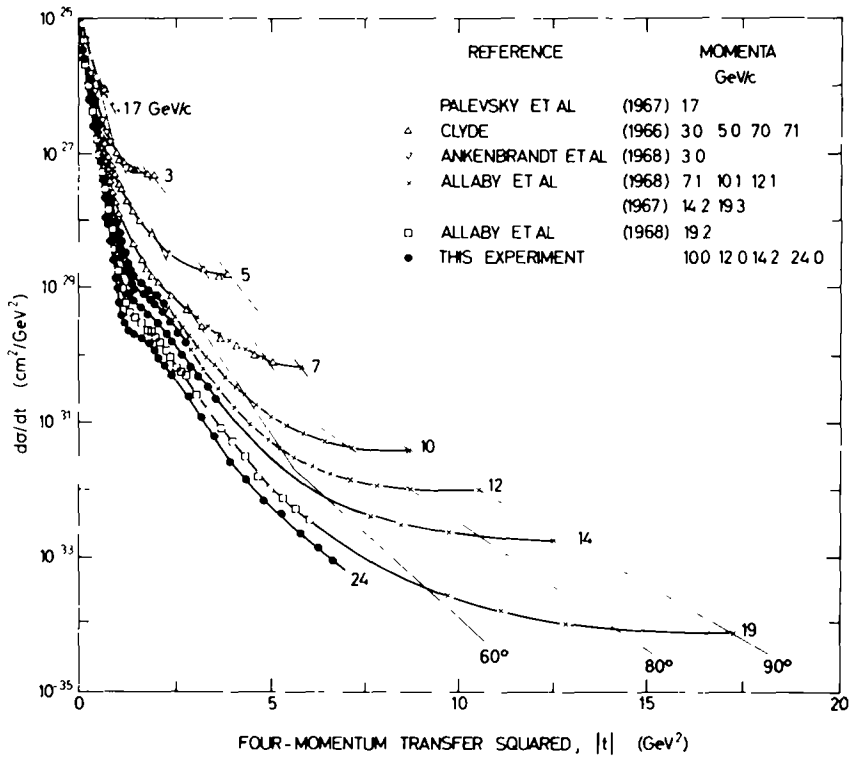
Fig. 12. Angular distributions for proton-proton elastic scattering over a range of four-momentum transfer larger than that shown in fig. 11. The data at the same incident momenta have been joined by a smooth curve. The loci of cross sections for fixed c.m. scattering angles are indicated for 60°, 80° and 90°. The data are taken from refs. [1, 18, 20, 53, 76, 78] and this experiment.

structure which was observed at 19.2 GeV/*c* at a |*t*| of 1.2 − 1.5 GeV² is present in the new data, from 10.0 to 24.0 GeV/*c*. The structure is not seen in the results of Clyde [76] at 5 and 7 GeV/*c*, nor in those of Brabson et al. [77] up to 5.5 GeV/*c*, hence it evidently becomes more pronounced with increase of energy, first developing between about 7 and 10 GeV/*c*.

Another presentation of the data is given in fig. 12, which covers a |*t*| range larger than that of fig. 11 in order to accommodate cross sections measured up to c.m. scattering angles of 90°. In addition fig. 12 indicates the loci of cross sections for fixed c.m. scattering angles. By this means the association, discussed in subsect. 2.3, of the 90° "break" in the cross section at around 8 GeV/*c* with the development of the structure at |*t*| ≃ 1.2 GeV² is clearly demonstrated.

The structure in pp elastic scattering is qualitatively different from that exhibited at lower incident momenta in $\pi^\pm p$, K⁻p and $\bar{p}p$ elastic scattering for |*t*| < 2 GeV².

FOUR-MOMENTUM TRANSFER SQUARED, |t| (GeV)
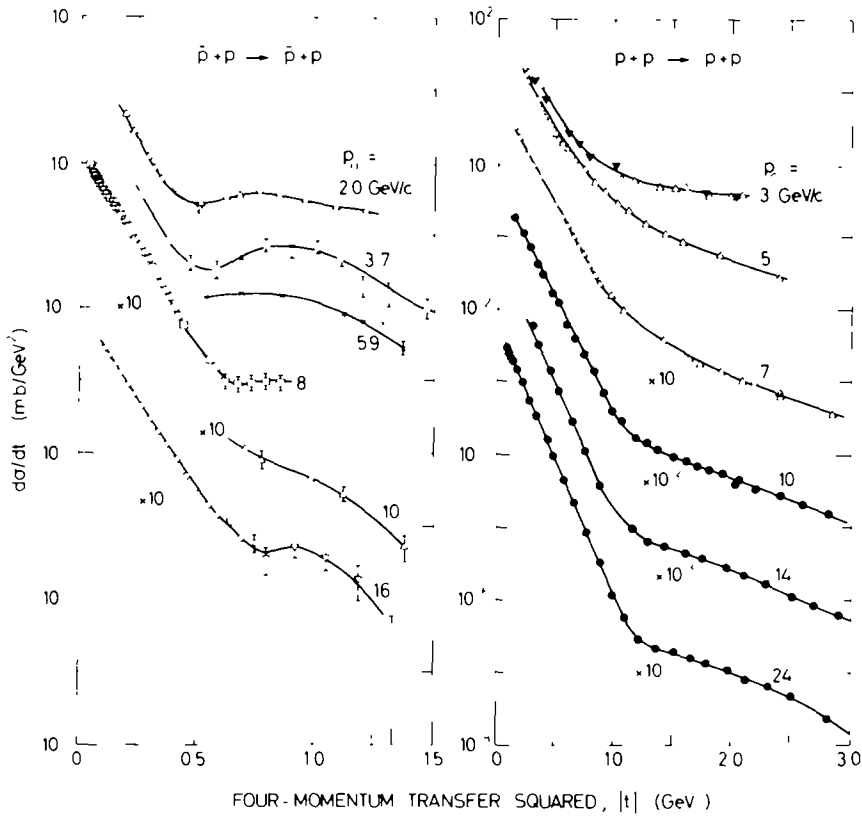
Fig. 13. A comparison of angular distributions of pp and pp elastic scattering. The antiproton data are from ref. [80] and the proton data from refs. [18, 20, 53, 76] and this experiment.

These latter structures, which tend to decrease with energy have been discussed in various ways and a strong connection has been made [79] with the operation of direct channel resonances which are absent in the pp system. Fig. 13, shows a comparison of the structure in the pp and in the pp [80] angular distributions and exhibits the difference in energy dependence. From considerations within the framework of the Pomeranchuk theorems, it might be expected that this difference will decrease with increasing energy until the angular distributions are the same under asymptotic conditions.

There is interest in the comparison of the form of the pp angular distribution with that of the angular dependence of pp polarisation $P_0(t)$. Measurements [81] with polarized targets have been made up to 17.5 GeV/c incident momentum over a range of |t| up to 2.5 GeV^2, so that a limited amount of data of reasonable precision is available for comparison. Fig. 14 shows comparisons of $d\sigma/dt$ and $P_0(t)$ around 6 GeV/c and at 10 GeV/c. At both these momenta the polarisation distribu-
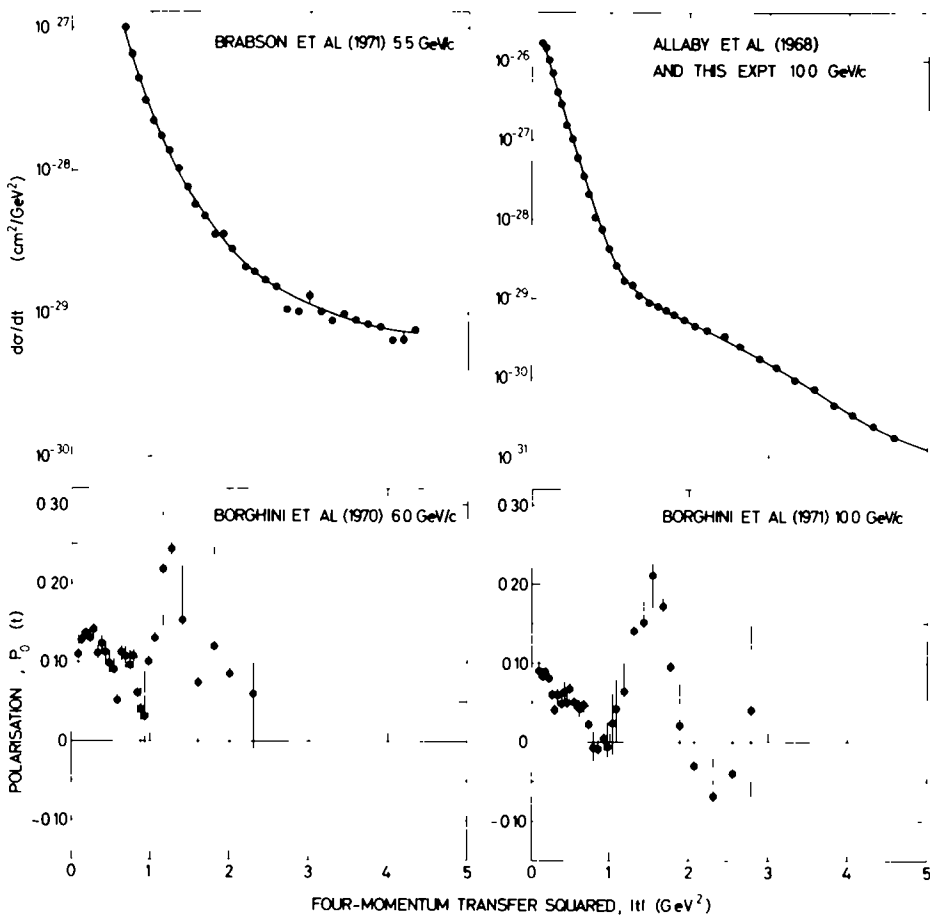
Fig. 14. A comparison between proton-proton elastic scattering (refs. [20, 77] and this experiment) and polarization (ref [81]) data near 6 and 10 GeV/c.

tion is qualitatively the same, exhibiting a dip or zero at $|t| \simeq 1$ GeV^2 and a peak at $|t| \simeq 1.5$ GeV^2. It seems, however, that the structure in $P_0(t)$ is a little more pronounced at 10 GeV/c than at the lower momentum, although the energy dependence of the polarisation structure is considerably less than that in the angular distribution in this region. Fig 14 shows that it may be concluded that the parts of the pp scattering amplitude (essentially "spin-orbit" contributions) which give rise to the polarisation exhibit momentum transfer dependent properties which are smoothed out in the angular distribution by other parts of the amplitude. The situation is thus rather different from that found, for example, in $\pi^{\pm}p$ scattering in which the "dip-bump" structure in both $P_0(t)$ and in $d\sigma/dt$ develop together. The

relationship of the "dip-bump" structure in $\pi^{\pm} p$ angular distributions and polarisations is well known and is well explained by duality considerations [79] through direct channel resonances. Such dynamics play no part in the pp system however.

It has been suggested [29, 82] that the pp differential cross section should approach asymptotically to $G^4(t)$, the fourth power of the electromagnetic form
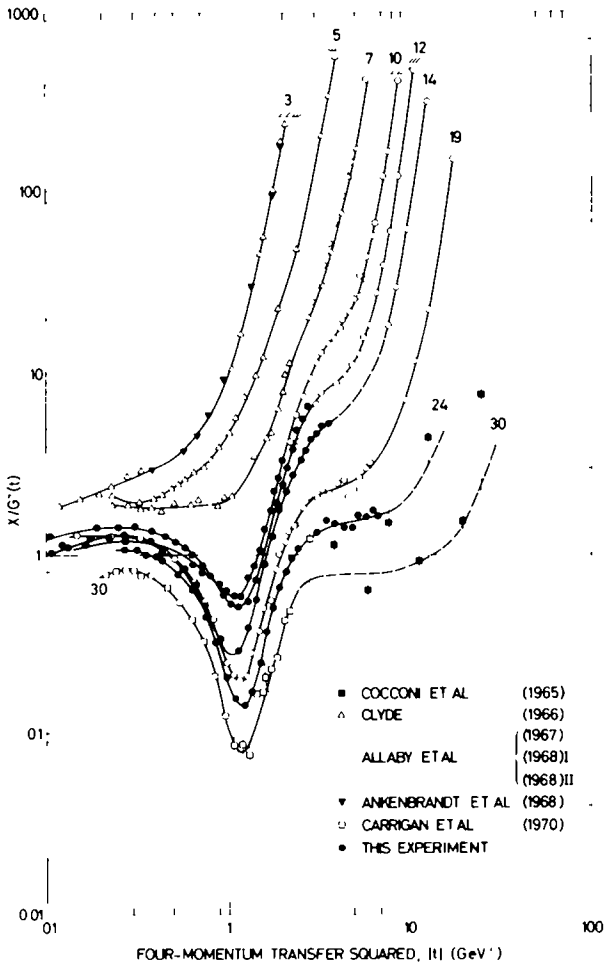
Fig. 15. A detailed comparison between measured differential cross sections and $G^4(t)$. The quantity X is the ratio of the differential cross section, $d\sigma/dt$, to the calculated optical theorem value in the forward direction. The figure shows X divided by $G^4(t)$ as a function of $|t|$. The lines drawn are merely to link the points corresponding to a fixed incident momentum, which is indicated at the end of each line. The symbol at the end of the curves corresponding to the low-energy data indicates 90° c.m. The data included in this figure are from refs [1, 12, 18, 20, 53, 76, 83] and this experiment.

factor of the proton. This function, normalised to the optical theorem value at 20 GeV/c, is shown with the pp data in fig. 11. For simplicity, the dipole form for $G(t)$ has been used

$$G(t) = (1 + |t|/0.71)^{-2} \,. \tag{12}$$

since the small deviations of the form factor data from the dipole form make no essential difference for this comparison. In fact, as seen in fig. 11 the pp angular distributions fall below $G^4(t)$ by about a factor ~ 10 in the region where the structure develops, and rise above $G^4(t)$ at larger momentum transfers. Nevertheless, the variation of $G^4(t)$ as expressed by eq. (12) does qualitatively follow the pp angular distributions over nine orders of magnitude. Thus, independent of any theoretical ideas, a comparison of the pp cross sections to the form of $G^4(t)$ is a convenient way of approximately removing the strong t-dependence of the angular distributions.
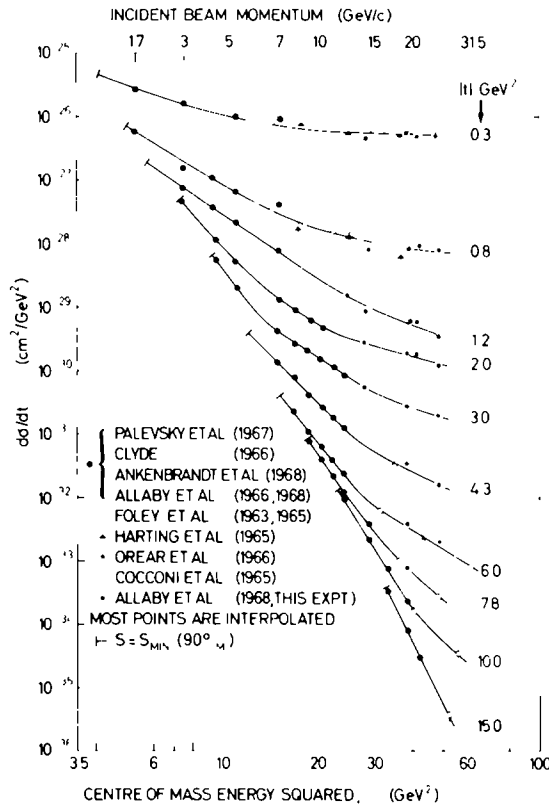
Fig. 16. The energy dependence of proton-proton elastic scattering at fixed values of four-momentum transfer squared t. The data in this figure are from refs [1, 12, 18, 20, 53, 76, 78, 84] and this experiment.

In fig. 15, a compilation of pp scattering data [1, 12, 18, 20, 53, 76, 83] is shown in the form of $X/G^4(t)$, where X is the ratio of the measured pp differential cross section $d\sigma/dt$ to the calculated optical theorem value in the forward direction. The development of the structure with incident momentum can more easily be seen. The most prominent feature is the sharp dip at $|t| = 1.2$ GeV^2 which develops at momenta above 7 GeV/c. At $|t|$ values above ~ 3 GeV^2 there is a flattening of the quantity $X/G^4(t)$ starting at 10 GeV/c and becoming more pronounced with increasing incident momentum. This feature of the angular distribution suggests the development of a second structure, slowly being revealed as the energy increases.

The energy dependence of the pp elastic scattering cross sections at fixed $|t|$ values is shown in fig. 16. The energy dependence in the diffraction region is not very strong, ($\sim \ln s$), however it rapidly develops, being approximately s^{-10} at $|t|$ = 15 GeV^2. If such a behaviour persists at much higher energies, the range of momenta transfer over which cross sections may be measured will be quite restricted. On the other hand, if the cross section at large s and t remains greater then $G^4(t)$, as suggested by various models, then the curves drawn in fig 16 might be expected to flatten at momentum transfers larger than so far explored.

5.1.2. Comparison of results with various models

In this section, pp elastic scattering angular distributions are compared with the results of some of the theoretical models outlined in subsect. 2 4. The comparison is meant to be illustrative rather than exhaustive.

Fig. 17a shows data at 5, 12 and 24 GeV/c together with results of an optical model calculation, by Durand and Lipes [30], using an impact parameter representation for the purely imaginary scattering amplitude (curve I). The matter distribution was assumed to be the same as the charge distribution determined by the electromagnetic form factor. As remarked in subsect. 2.4.3 the resulting angular distribution is supposed to be asymptotic. A modification to this, by the inclusion of a small real part in the amplitude, is also shown (curve II) The calculated distributions exhibit diffraction zeros or minima in the vicinity of the structure in the experimental results, a possible second structure, developing with energy, is also seen in the data of fig 15

Fig. 17b gives the results of another type of optical model by Cheng et al. [30], fitted to data at 5, 10 and 19.2 GeV/c. In this model an impact parameter formulation was employed to describe diffraction scattering from a grey, absorbing region of radius about 0.7 0.8 fm together with peripheral or resonant scattering from the surface of the absorbing sphere. The components of the scattering amplitude were varied with energy to fit the angular distribution, the polarisation, the total cross section and the phase of the forward scattering amplitude. This model leads to a diffraction-type structure which develops with energy as the real part of the amplitude, which effectively fills up the dips at low energies, decreases. For the overall fit in this model, 13 adjustable parameters are required at each energy.
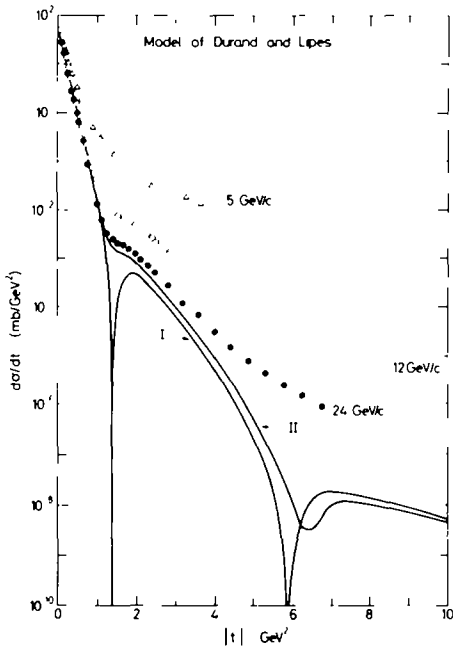
I ig. 17a. A comparison of the results of the model of Durand and Lipes [30] with experimental data shown in fig. 11. Curve I is the result for an asymptotic purely-imaginary scattering amplitude while curve II shows the effect of including a small real part in the amplitude.
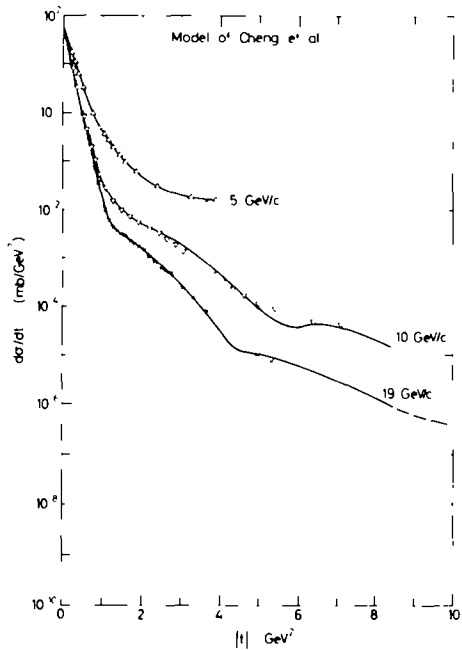
I ig 17b A fit of the model of Cheng et al [30] to data from the collection of fig 11

In fig. 17c the results of the hybrid model of Chiu and Finkelstein [36] are compared with the data at 5, 12 and 24 GeV/c. This model takes seriously the asymptotic distribution of Durand and Lipes [30] or Chou and Yang [30] and identifies it, dynamically, as generated by a fixed Pomeranchuk pole and cuts. In addition an energy dependence is introduced, for non-asymptotic energies, by means of the normal, moving, pole contributions of the exchange-degenerate ω and f^0 trajectories and their cuts. While not particularly successful, apart from indications of the structure, this model at least provides a means of relating the present experiments to a possible limiting distribution, if it exists.

The Regge-pole model of Frautschi and Margolis [37] is based upon a moving Pomeranchuk pole (slope = 0.82 GeV ^{2}) and its iterations or cuts, the formalism used being that of the Glauber expansion leading to multiple exchange terms. The results of the calculation are given in fig. 17d together with data at 5, 10 and 24 GeV/c. The model indicates a shift of the diffraction minima to lower momentum transfer as the energy is increased and a steady fall in cross section at fixed $|t|$ due
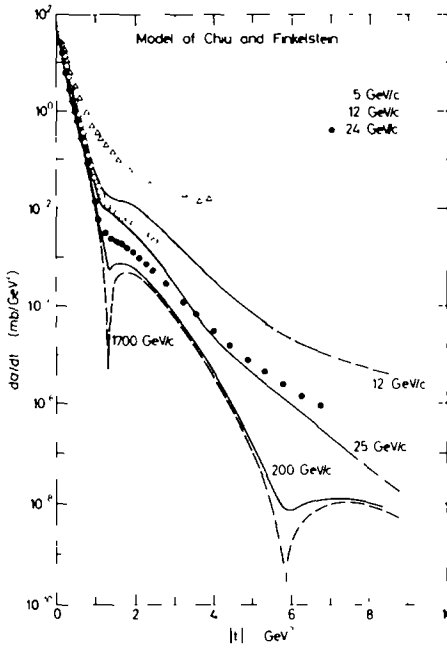
I ig. 17c. Results of the model of Chiu and Finkelstein [36] compared with experimental data displayed in fig. 11.
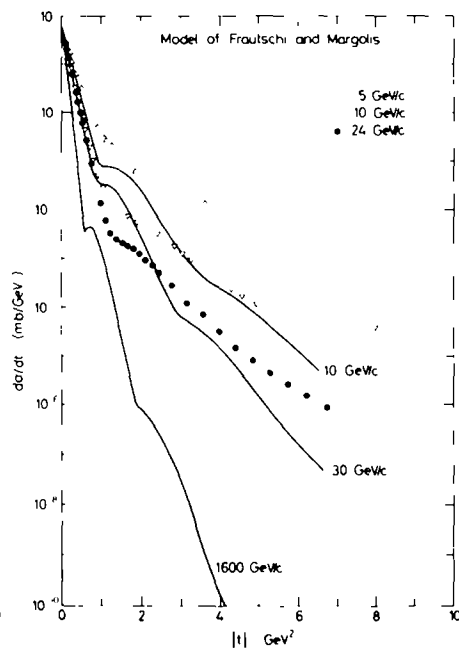
I ig. 17d. A comparison of the results of the model of Frautschi and Margolis [37] with data shown in fig. 11.

to the characteristic energy-dependence of a moving pole. In addition a slowly rising pp total cross section is predicted

I ig. 17e shows a fit of the model of Greco [38] to data at 7, 10 and 19 GeV/c. In this approach the Pomeranchuk pole and its cuts are considered as dual [79] to non-resonating background in the scattering amplitude. A Veneziano [39] formula is used to describe the pole and cut terms in the scattering amplitude. As can be seen in fig. 17e, the fit to the data is good and the energy dependence, as shown by the predicted distribution at 58 GeV/c, is rather strong. The slope of the Pomeranchuk pole is found to be 0.90 GeV^{-1} and the total cross section is predicted to decrease asymptotically to about 30 mb.

Finally, fig 17f shows the results of the calculation of Abarbanel et al [40] with data at 5, 12 and 24 GeV/c. The calculation, based on the dominance of a new current-current interaction over a diffractive Regge pole-like tail, was performed so as to obey unitarity and required to approach within a constant factor the fourth power of the electromagnetic form factor. A smooth dependence on momentum transfer results (curve 1). Abarbanel et al. [40] have remarked that the optical model calculation of Durand and Lipes [30] did not satisfy unitarity. Consequently Abarbanel et al. have carried through the Durand and Lipes model
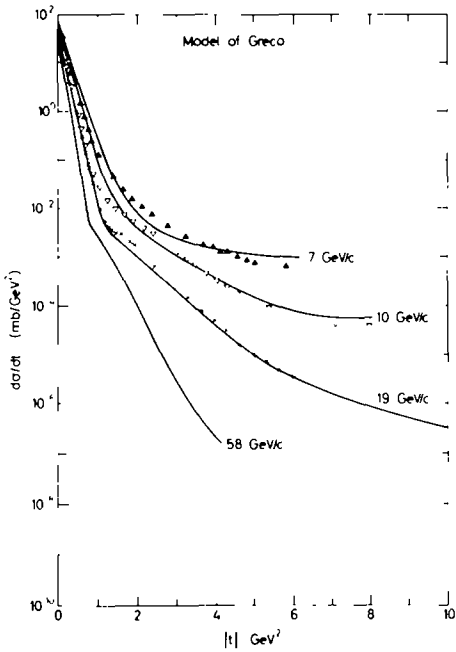
Fig. 17e. A fit of the model of Greco [38] to experimental data shown in fig. 11. A prediction for 58 GeV/c is also shown.
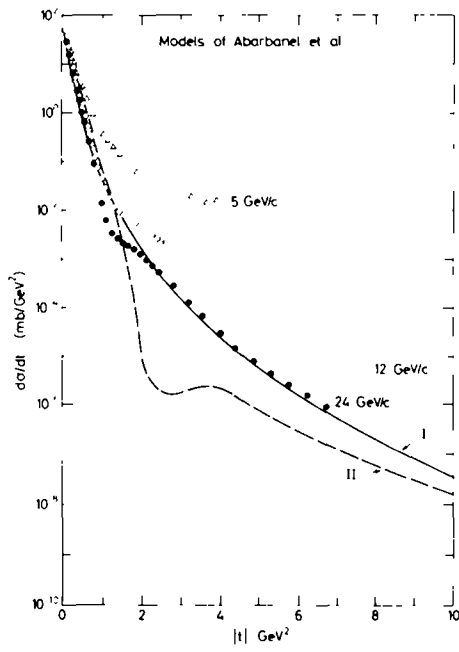
Fig. 17f. A comparison of experimental data with the results of calculations of Abarbanel et al. [40]. Curve I shows their current-current model results, while curve II is a unitarised version of the Durand and Lipes [30] model.

requiring this condition. The result is shown in fig. 17f (curve II) which, on comparison with fig. 17a, indicates a strong damping of the diffraction structure.

All of the models discussed above apart from the special one of Abarbanel et al [40], share the common feature that they may be formally interpreted (see a review of Jackson [21]) in terms of a multiple scattering mechanism in which one attempts to understand the angular distribution structure as due to transitions between different orders of scattering (i e. from single to double, etc.) by analogy with the scattering of composite systems. In this interpretation such structure would be expected to be a common property of all hadron-hadron scattering processes.

5.2. Inelastic proton-proton scattering

The present experiment at 24.0 GeV/c exhibits several characteristic features of the process $p + p \rightarrow p + X$, where X is a nucleon resonance or a continuum state. The differential production cross sections of the resonances are given in table 3 and their angular distributions are summarized in fig. 18. The various points exhibited in fig. 18 are now discussed and compared with the situation at other energies.
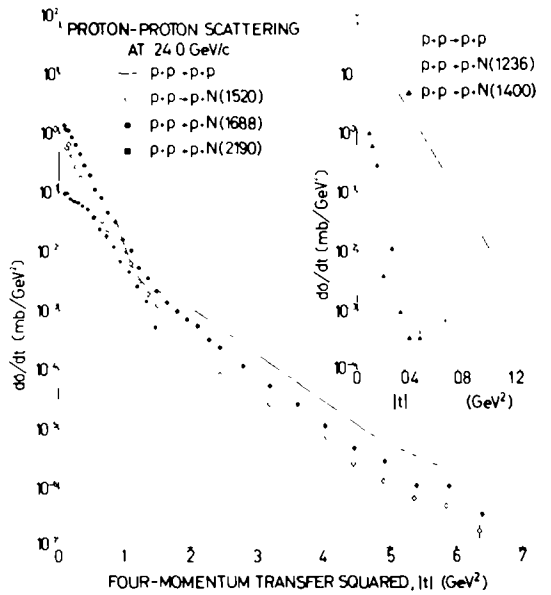
Fig. 18. Differential cross sections for nucleon resonance production and elastic scattering in 24.0 GeV/c proton-proton interactions. The symbol used for the last points of the N(1400) cross section represents a one standard deviation upper limit.
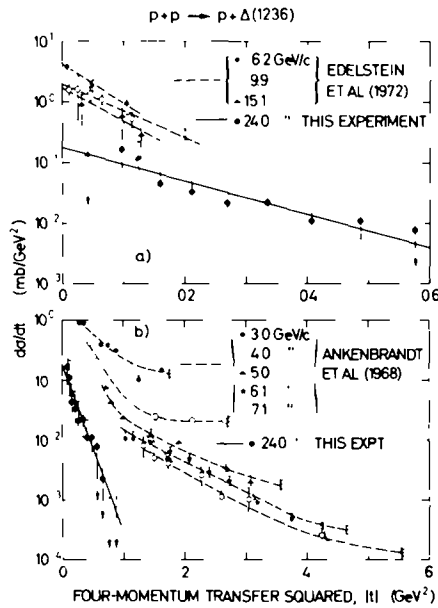
Fig. 19. Differential cross section for the production of the Δ(1236) resonance in proton-proton interactions. The present data at 24.0 GeV/c are plotted together with data from lower energies, refs. [50, 53].

5.2.1. General features of resonance excitation and comparison with data at other energies

At small $|t|$, around 0.1 GeV^2, the N(1400), N(1520) and N(1688) are excited rather strongly and with comparable cross sections. The Δ(1236) and N(2190) are also observed in this region of $|t|$ but are produced less strongly ($\sim \frac{1}{10}$) than the other three states. The momentum transfer distributions $d\sigma/dt$ for the Δ and N resonances are given in figs. 19−23.

It is customary to fit the angular dependence of nucleon resonance production at small to moderate four-momentum transfers by the formula

$$\frac{d\sigma}{dt} = \left(\frac{d\sigma}{dt}\right)_{t=0} \exp\left(-B|t|\right). \tag{13}$$
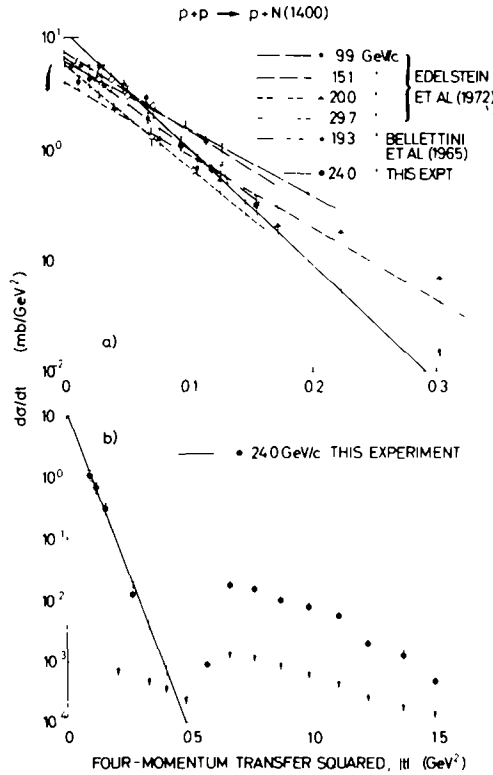
Fig. 20. Differential cross section for the production of the N(1400) resonance in proton-proton collisions. In (a) the data of this experiment at 24.0 GeV/c are compared with other published results (refs. [48, 50]). In (b) the data from this experiment up to $|t| = 1.5$ GeV^2 are shown. The broken lines on the data points at $|t| \gtrsim 0.5$ GeV^2 represent the additional uncertainty in the cross sections due to the possible ambiguity in the fitting procedure (see subsect. 4.2).

p + p ⟶ p + N(1520)
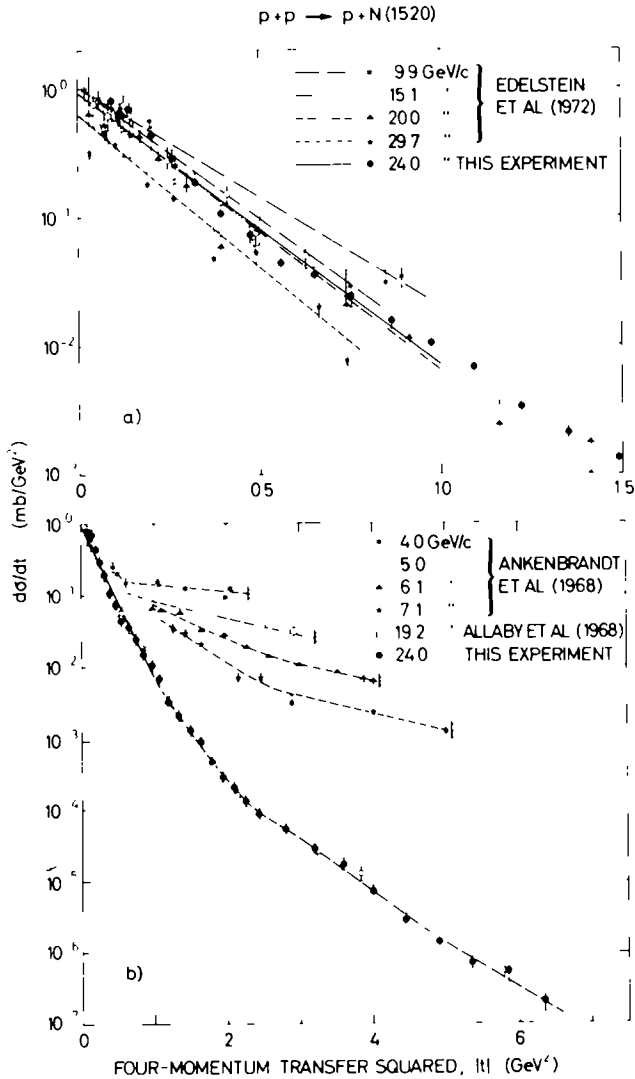
Fig. 21. The differential cross section for the production of the N(1520) in proton-proton collisions at 24.0 GeV/c is compared with the available published data (refs. [50, 53, 54]).

The total cross sections σ are obtained by integrating eq. (13) and multiplying by a factor 2 to take account of both target and projectile excitations. Hence

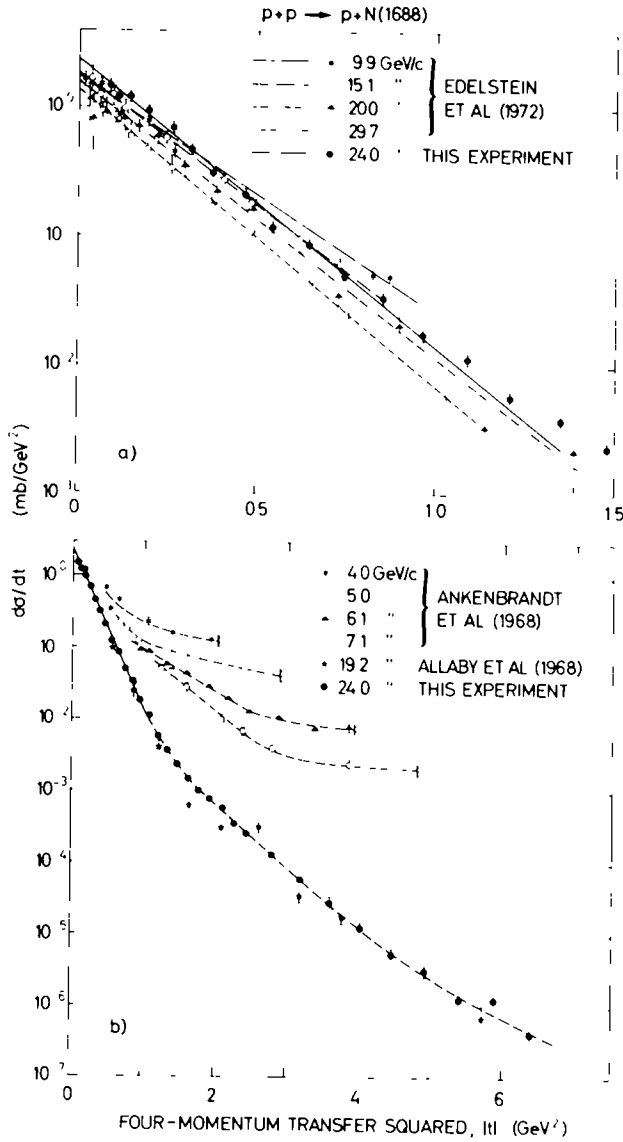$$\sigma = \frac{2}{B} \left(\frac{d\sigma}{dt} \right)_{t-0} . \tag{14}$$

Fig. 22. The cross section for the production of the N(1688) resonance in proton-proton collisions at 24.0 GeV/c is shown with other published data (refs. [50, 53, 54]).

The measured distributions have been fitted using eq. (13), and the values found for the slope parameter B, the cross section $(d\sigma/dt)_{t=0}$ and the range of $|t|$ used in the fit are given in table 5 for each resonance. The isospin $\frac{1}{2}$ states exhibit a certain
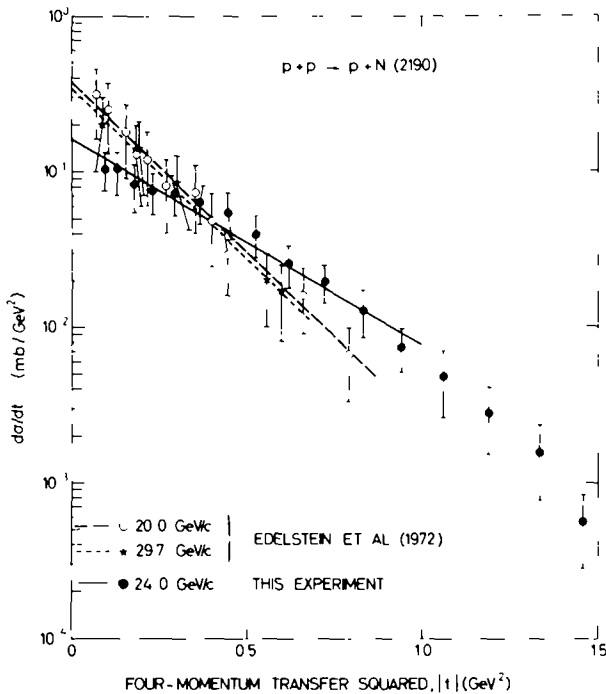
I ig. 23. The cross section for the production of the N(2190) resonance in proton-proton interactions at 24.0 GeV/c is compared with the data of Edelstein et al. [50].

systematic order in the steepness of their angular distribution in that, on the average, the heavier masses appear to have smaller slopes.

The angular distribution parameters of eq. (13) and the total cross sections are given in fig. 24 for the Δ(1236) and in fig. 25 for the N resonances. These figures exhibit the well-known energy dependence of isospin exchanging processes for the Δ(1236), and the energy independence of the N states characterising diffraction dissociation.

The large uncertainties associated with the N(1400) and Δ(1236) data are caused by the difficulties of extracting these cross sections from the spectra. On the one hand the N(1400) is very close to the N(1520) and has a very steep angular distribution, and on the other the Δ(1236) appears between the elastic and N(1400) peaks and has a small cross section due to the suppression [55, 56] at high energies of scattering mechanisms involving isospin exchange.

The large errors in the Δ(1236) cross section as measured in the present experiment render any comment uncertain, however figs. 19 and 24 show the general features. The angular distributions are qualitatively similar to those of the other resonances, while $(d\sigma/dt)_{t=0}$ and hence the total cross section decreases strongly with

Table 5

The slope parameter B, intercept $(d\sigma/dt)_{t=0}$ and total cross section σ values derived from the resonance production results at 24.0 GeV/c and using eqs. (13) and (14)

Resonance	$|t|$ range (GeV^2)	Slope B (GeV^{-2})	$(d\sigma/dt)_{t=0}$ (mb/GeV^2)	σ (mb)
$\Delta(1236)$	0.099 – 0.666	6.4 ± 0.8	0.18 ± 0.05	0.057 ± 0.017
N(1400)	0.094 – 0.264	24.2 ± 2.5	11.6 ± 4.2	0.96 ± 0.35
N(1520)	0.091 – 0.973	4.84 ± 0.24	0.91 ± 0.19	0.37 ± 0.07
N(1688)	0.087 – 0.965	5.12 ± 0.08	2.35 ± 0.36	0.92 ± 0.14
N(2190)	0.097 – 0.941	3.01 ± 0.17	0.16 ± 0.05	0.108 ± 0.033

The quoted errors include the effect of the ± 15% systematic error in the cross section measurements, except for the N(2190) where the systematic error is ± 30%.

energy. These facts are consistent with what is known about $\Delta(1236)$ production in bubble chamber experiments [85]*.

The cross sections for the production of the N(1400) are shown in fig. 20. Results obtained by applying the present fitting procedure to the published spectra of Bellettini et al. [48] are shown in the figure and are also listed in table 6. The present data at 24.0 GeV/c are in good agreement with the previous measurements in reproducing the fast drop of the differential cross section as $|t|$ is increased. In fig. 20 the results for $|t| > 0.5$ GeV^2 are plotted with the error bars resulting from the fitting procedure. The broken lines indicate the additional uncertainty in the cross sections due to the possible ambiguity in the fitting procedure at large $|t|$. This region of momentum transfer was not covered in previous experiments. Due to the difficulty in extracting the N(1400) cross sections, expecially for $|t| > 0.5$ GeV^2, these results can only be regarded as a suggestion of a second diffraction-like maximum which may be developing.

The $|t|$-dependences of the N(1520) and the N(1688) are very similar over the whole range studied (figs. 21 and 22). Above $|t| = 2$ GeV^2 the distributions are also very similar to that for elastic scattering. This feature suggests a common mechanism for elastic scattering and N(1520) and N(1688) production at large momentum transfers. The elastic scattering structure at $|t| \simeq 1.5$ GeV^2, dividing the steep forward peak ($B \simeq 10$ GeV^{-2}) from the large momentum transfer scattering, is not

---

* The present data are also in agreement with the recent and more accurate results at 17 GeV/c on the reaction p + p → $\Delta(1236)$ + n, reported by G. Grayer et al. at the Batavia Conference in September 1972.

Table 6

Resonance production cross sections in proton-proton collisions at 19.3 GeV/c by Bellettini et al. [48] which have been extracted using eq. (10) of this paper

Range of angles θ_{lab} (mrad)	N(1400)		N(1520)		N(1688)	
	$\lvert t \rvert$ (GeV²)	$d\sigma/dt$ (cm²/GeV²)	$\lvert t \rvert$ (GeV²)	$d\sigma/dt$ (cm²/GeV²)	$\lvert t \rvert$ (GeV²)	$d\sigma/dt$ (cm²/GeV²)
2 – 4	0.0045	(5.3 ± 0.5) E-27	0.0050	(8.5 ± 3.6) E-28	0.0065	(1.23 ± 0.34) E-27
4 – 7	0.013	(5.6 ± 0.4) E-27	0.013	(3.5 ± 3.2) E-28	0.014	(1.26 ± 0.34) E-27
7 – 11	0.032	(3.7 ± 0.3) E-27	0.032	(7.3 ± 3.2) E-28	0.033	(9.8 ± 3.8) E-28
11 – 15	0.067	(1.9 ± 0.2) E-27	0.067	(4.8 ± 1.5) E-28	0.068	(7.1 ± 2.0) E-28
15 – 19	0.106	(6.7 ± 2.3) E-28	0.106	(9.2 ± 2.2) E-28	0.106	(9.6 ± 2.5) E-28

The data are for a range of lab angles of the forward-scattered protons. The value of four-momentum transfer squared at the mean angle of this range is quoted. The errors shown in the table are statistical; the systematic uncertainty in the data is estimated to be always less than the statistical error. The N(1400) resonance production cross sections were fitted using eqs. (13) and (14) over the $\lvert t \rvert$ range from 0.004 – 0.106 GeV², and produced the following results: slope $B = 18.8 \pm 2.2$ GeV^{-2}, intercept $(d\sigma/dt)_{t=0} = 6.6 \pm 0.5$ mb/GeV², $\sigma = 0.70 \pm 0.08$ mb.
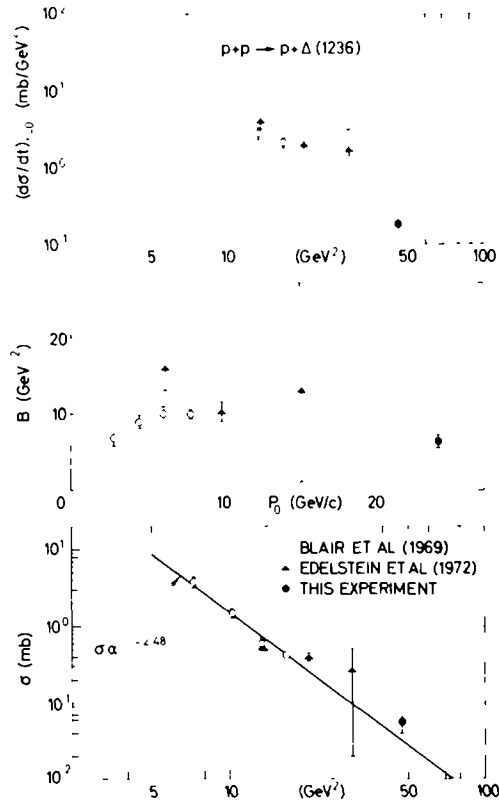
Fig. 24. The total cross section σ for $\Delta(1236)$ production as a function of incident momentum. The data from this experiment at 24.0 GeV/c are shown with other published results [50, 51]. The slope parameter B and intercept $(d\sigma/dt)_{t=0}$ are defined in eq. (13).

found in the resonance distributions, which exhibit very smooth $|t|$ dependences. With respect to energy dependence it is seen that the angular distributions have only a weak s-dependence at small $|t|$, and a very strong one at large momentum transfer. From fig. 25, it is seen that the forward cross sections, and consequently the total cross sections, are essentially energy independent.

The data at 24.0 GeV/c on the production of the N(2190) up to $|t| \simeq 1.5$ GeV^2 are shown in fig. 23 together with the results of Edelstein et al. [50] at 20 0 and 29.7 GeV/c. As the two angular distributions are, within the errors, the same, it should be expected that the 24.0 GeV/c data should have at least the same slope. Fig. 23 shows that this is not so, thereby indicating some systematic difference between the two experiments in their extraction of the N(2190) cross section.

At 24.0 GeV/c it may be observed that the N(1520), N(1688), N(2190) and elastic cross sections are all comparable around $|t| \simeq 1.5$ GeV^2.
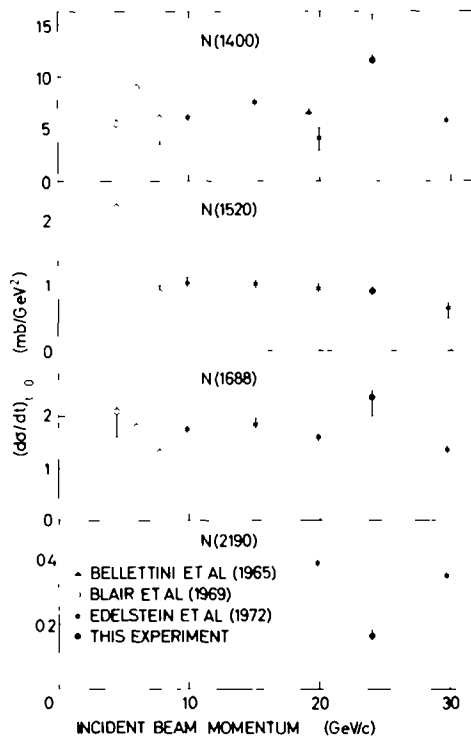
Fig. 25a. The momentum dependence of the forward production cross sections $(d\sigma/dt)_{t=0}$, defined in eq. (13), of the isospin $\frac{1}{2}$ resonances. The data are from refs. [48, 50, 51] and the present experiment.

5.2.2. Comparison of N(1688) production with elastic scattering

The N(1688) production cross section was determined with less ambiguity than the other resonances because of the prominence of the peak in the measured spectra. In fig. 26 the ratio of N(1688) production to elastic pp scattering is compared with the same ratio for corresponding reactions initiated by 16 GeV/c negative pions [86, 87], and by high-energy electrons [75]. In the region $0 \leqslant |t| \leqslant 0.5$ GeV^2 the ratios for π^-p and pp are essentially the same [86] in support of the idea of factorization of the Pomeranchuk singularity [88], that is, the production cross sections satisfy the relation

$$\frac{\pi p \to \pi N(1688)}{\pi p \to \pi p} = \frac{pp \to pN(1688)}{pp \to pp} . \tag{15}$$

For $|t|$ values between 0.5 and 1.5 GeV^2 the ratio for the proton-initiated reactions is larger, showing a peak which reflects the structure in the elastic cross section. Beyond $|t| = 2$ GeV^2 the ratios for the pp and ep data are similar, as conjectured by
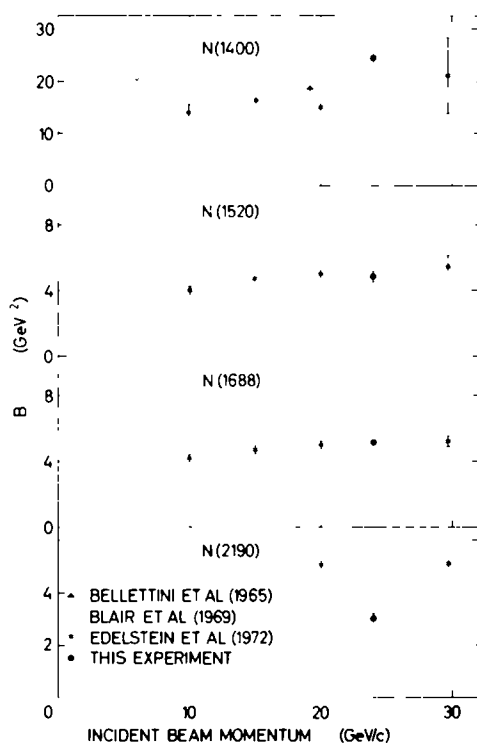
Fig. 25b. The momentum dependence of the slope parameter B, defined in eq. (13), for the production of the isospin $\frac{1}{2}$ resonances. The data are from the present experiment at 24.0 GeV/c and from refs. [48, 50, 51].

Wu and Yang [29]. In addition, as has already been noticed by Anderson et al. [86], fig. 26 shows that the π p and ep ratios are similar over their whole common range of momentum transfer.

5.2.3. Comparison of resonance and background momentum transfer distribution

Fig. 27 shows the elastic, the N(1520) and N(1688) angular distributions together with continuum cross sections for missing masses of 1.5, 2.0 and 2.5 GeV. The continuum cross sections were calculated from the polynomial expression in eq. (10) and normalised to a missing mass interval of 1.0 GeV according to eq. (11). In addition an estimate was made of the contribution in the non-resonant background continuum due to protons produced *via* the decay of excited projectile protons. The results of a Monte-Carlo calculation, which made use of the measured angular distributions for the N(1520), N(1688) and N(2190) resonances, are shown in fig. 28. The calculated contribution of the decay protons in the non-resonant background in the region of the N(1688), for example, varied from 0.8 to 3.0% as $|t|$ varied from
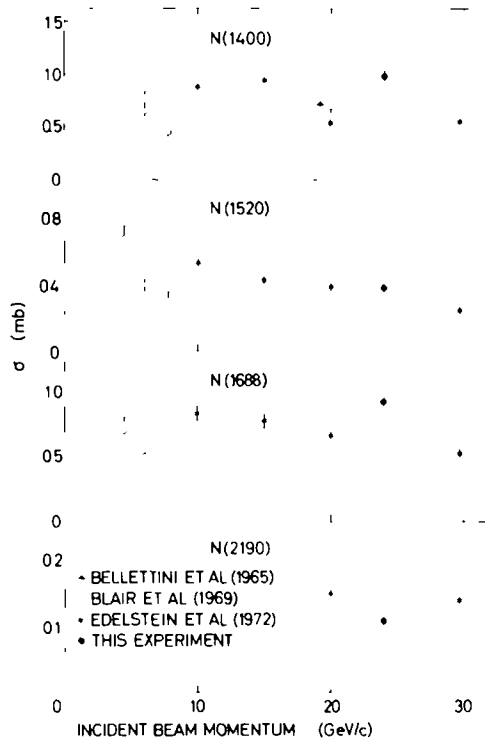
Fig. 25c. The total cross sections σ for the production of the isospin $\frac{1}{2}$ resonances as a function of incident momentum. The data from the present experiment at 24.0 GeV/c are shown with the other published results [48, 50, 51].

0.1 to 3.0 GeV^2. It was therefore concluded that projectile excitation could give only a small contribution to the continuum spectrum in comparison to target break-up. As a general point [70, 89], and consistent with that made for the isospin $\frac{1}{2}$ reso-nances in subsect. 5.2 1, fig. 27 shows that the angular distributions become flatter as the produced mass increases. This is a well-known and significant effect [75, 90] in electron-proton inelastic scattering.

The energy dependence of the background at large |t| is very similar to the energy dependence of the $I = \frac{1}{2}$ resonances, and thus also similar to that for elastic scattering. This may be contrasted with the results of previous measurements [50], at small |t|, which indicate that the non-resonant contributions to the missing mass spectra have a dependence of s^{-1}. The present data are compatible with such a trend. Various theoretical studies [91] involving the triple-Pomeranchuk vertex indicate that the energy dependence implies that the triple-pomeron coupling is small.

Another method of comparison of resonance and background cross sections, for specifically the N(1688), is shown in fig. 29 where the ratio of the N(1688) produc-
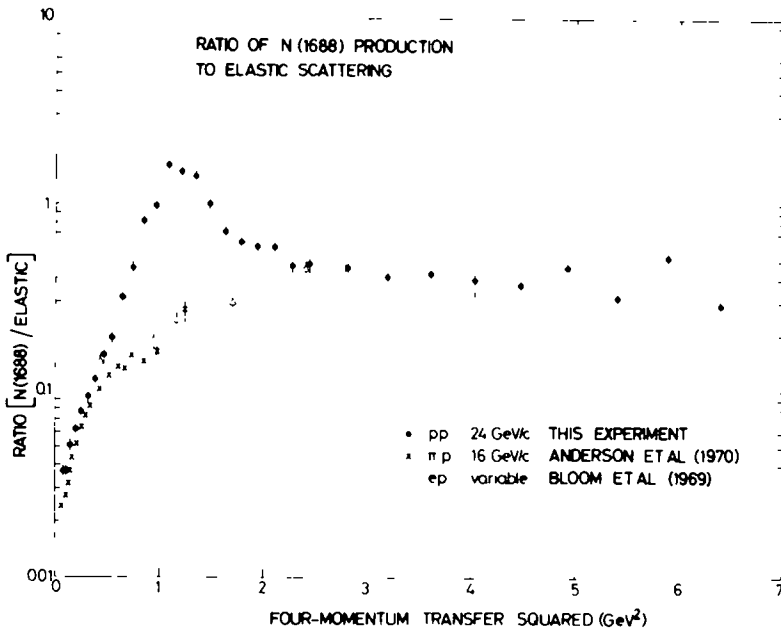
Fig. 26. The ratio of N(1688) production to elastic scattering is shown as a function of the four-momentum transfer squared, |t|, for 24 GeV/c pp collisions (this experiment), 16 GeV/c π⁻p collisions [86] and high energy ep collisions [75].

tion to the non-resonant production cross section in the same mass range is given as a function of $|t|$. As $|t|$ increases, this ratio has an initial fast rise and then a fall-off with a superimposed structure in the region $1 \leqslant |t| \leqslant 2$ GeV² It is not clear from the figure whether the ratio is levelling off to a finite value at large $|t|$, or proceeding towards zero. It has been speculated [92] that a large momentum transfers the relative importance of the process in which the nucleon breaks up into many fragments increases with respect to the occurrence of quasi-two-body processes. This idea is in qualitative agreement with fig. 29.

5.2.4. A phenomenological description of nucleon resonance production

The various models (subsect. 2.5.3) used until now to describe nucleon resonance production give neither a good description of the shapes of the angular distributions nor of the total cross sections. Hence a summary of the results of some of the calculations, in the style of that given (subsect. 5.1.2) for elastic scattering, will not be presented here. Instead, a discussion by Elitzur [62] on the relationship between the isospin $\frac{1}{2}$ resonance production and elastic scattering will be summarized.

The basis is essentially an optical model in which the cross section is related to the product of the form factors of the matter distributions of the colliding particles.
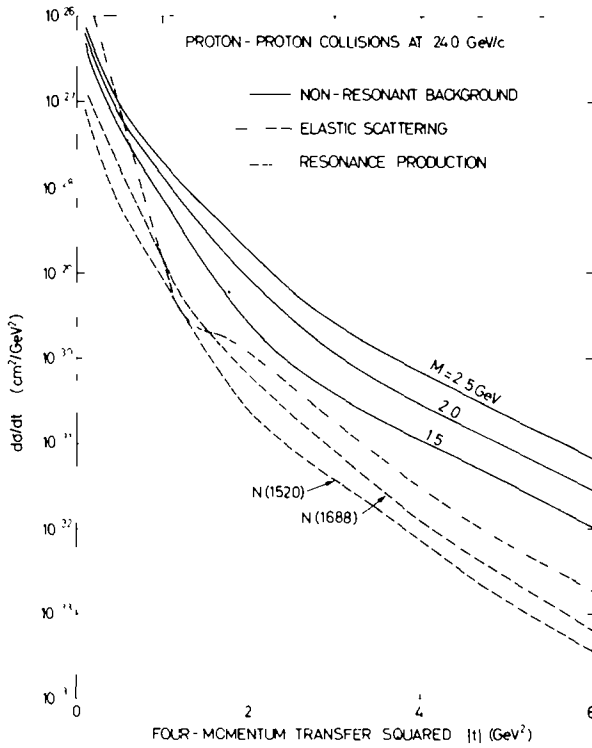
Fig. 27. The production cross section for non-resonant background (integrated over a missing mass interval of 1.0 GeV) in proton-proton collisions at 24.0 GeV/c is compared with the elastic and resonance production cross sections.

The suggestion of Wu and Yang [29] is then used to identify the form of the matter distribution with the electromagnetic form factor. It is then conjectured on the grounds of an analysis of Bloom and Gilman [93] that the electromagnetic form factors of all the resonances are given by one function, namely the electromagnetic elastic form factor, when written in terms of the variable $|t|/M^{*2}$ (where M^* is the resonance mass). These ideas lead immediately to the relationship

$$\frac{d\sigma_{pN}(t)}{dt} = \text{const} \left[\frac{d\sigma_{el}(t)}{dt} \frac{d\sigma_{el}(t^*)}{dt} \right]^{\frac{1}{2}} , \tag{16}$$

where $t^* = t(M/M^*)^2$. Furthermore, assuming that the forward scattering peak is exponential in terms of $|t|$, the slope parameter B for isospin $I = \frac{1}{2}$ resonance production [eq. (13)] is related to that for elastic scattering, b, [eq. (2)] by

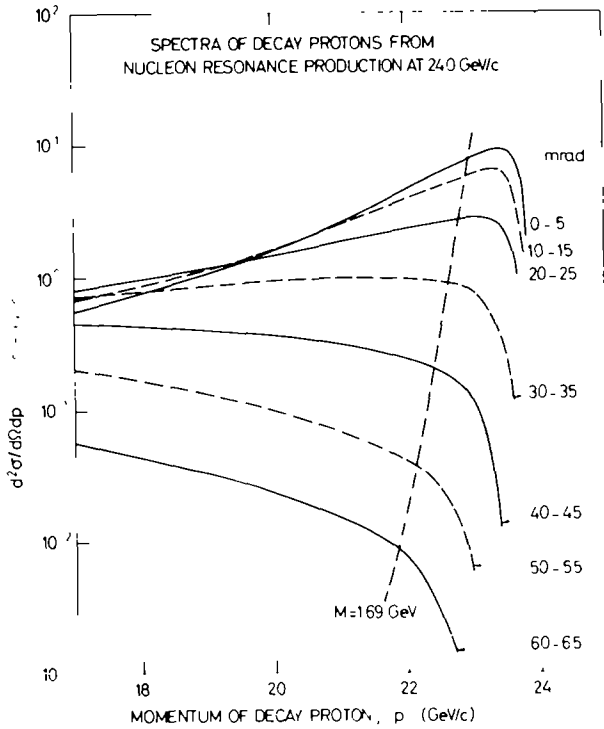$$B = \frac{1}{2} b \left[1 + (M/M^*)^2 \right] . \tag{18}$$

Fig. 28. The results of a Monte-Carlo calculation of the contribution in the non-resonance background continuum due to protons produced in the decay of excited projectile protons. The present measurements of the N(1520), N(1688) and N(2190) angular distributions have been used in the calculations.

Thus the forward angular distributions for the nucleon resonance production are expected to be much flatter than that for elastic scattering, the slope parameter differing by about a factor $\leqslant 2$, qualitatively in agreement with the data.

Fig. 30 shows the results of evaluating eq. (16) at 24 GeV/c using the 24 GeV/c elastic scattering data as input with arbitrary normalisation factors for the excitations of the N(1520), N(1688) and N(2190). The shapes of the N(1520) and N(1688) distributions are quite well reproduced but that for the N(2190) less well. The dependence predicted for this resonance is steeper than that observed at 24 GeV/c although, as indicated in subsect. 5.2.1, the data of Edelstein et al. [50] at 20.0 and 29.7 GeV/c would be more in accord with the predicted trend.

The N(1400) does not fit at all into the scheme described by eq. (16) as the slope parameter B for this resonance is more than a factor 2 bigger than that for elastic scattering. Apart from its rather constant total cross section the least massive of the isospin $\frac{1}{2}$ states has always appeared to possess different excitation characteristics from the other N resonances and thus remains particularly worthy of further study.
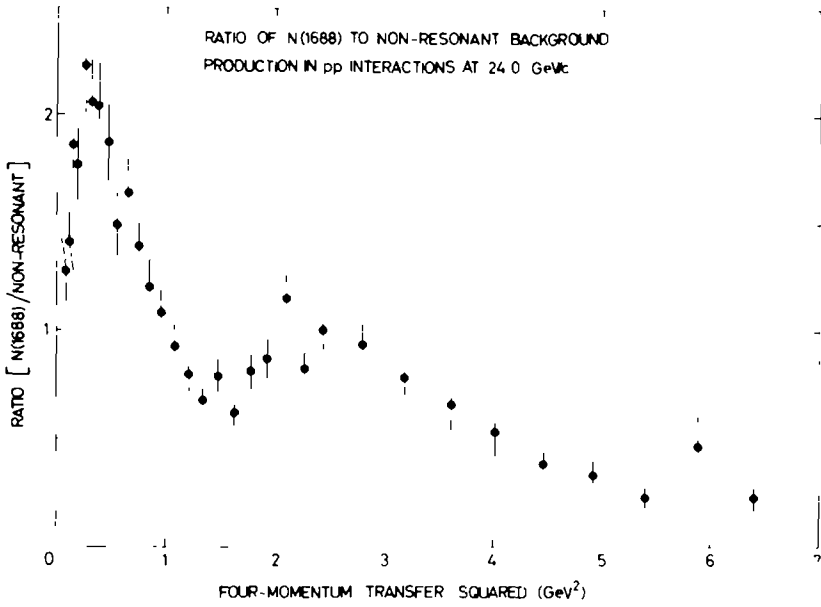
Fig. 29. The ratio of N(1688) to non-resonant continuum production in 24 GeV/c pp reactions (this experiment). The non-resonant continuum cross section has been integrated between the missing mass limits of 1.61 and 1.78 GeV.
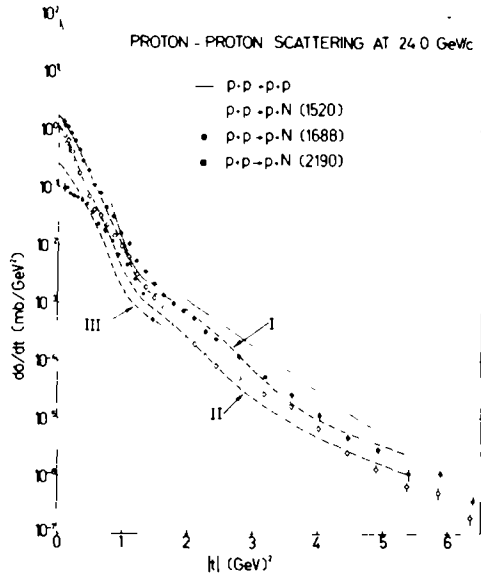

Fig. 30. A comparison of the model of Fitzur [62] for isospin $I = \frac{1}{2}$ resonance production (eq. (16)) and the experimental data at 24.0 GeV/c. Curves I, II and III denote the predictions for the N(1688), N(1520) and N(2190), respectively.

To conclude, it appears that, in spite of the detailed shortcomings of this phenom-enological description, the relations (16) and (17) are useful in correlating elastic and inelastic pp data.

6. Conclusions

6.1. Elastic scattering

(i) The main new results of the present experiment concern the development of structure in the pp angular distribution. Together with data at incident momenta up to 7 GeV/c, the results show that a shoulder in dσ/dt at a $|t|$ of 1.2   1.5 GeV^2 develops rather suddenly between 7 and 10 GeV/c. It is manifested also in the form of a sharp break [19] in the energy dependence of the 90° cross section and in the angular distribution [18] near to 90° at the incident momentum of 8 5 GeV/c. Be-tween 10 GeV/c and 30 GeV/c the structure changes little in form, although there is a slight increase in its prominence, as may be judged from figs 11 and 15*. Over the momentum range available it seems clear that the shoulder remains at a fixed four-momentum transfer. In addition, fig. 15 indicates the possibility of the devel-opment of a second structure at fixed $|t| \simeq 5$ GeV^2, although the evidence is rather inconclusive

(ii) A comparison of polarisation data with the angular distribution at the same energy shows that the "dip-bump" structure in $P_0(t)$ develops at lower energies than the shoulder in the angular distribution (fig. 14) There is not, therefore, an overall one-to-one relationship between the P_0 structure and that in dσ/dt as there is in, for example, π^+p scattering. In addition the energy dependence of the pp structure in dσ/dt differs completely from that for $\pi^\pm$p in that it develops with energy, starting around 8 GeV/c, while the phenomenon in the $\pi^\pm$p system at $|t| \sim 1$ GeV^2 declines with energy so far as it is measured up to $\simeq 20$ GeV/c. The comparison of the pp and pp angular distributions shown in fig 13 may be viewed in a similar manner

(iii) Another aspect of the nucleon-nucleon angular distribution structure is its isospin independence. Measurements [68] of elastic proton-neutron scattering at 24 0 GeV/c up to $|t| \approx 6$ GeV^2 show that the pn angular distribution follows the pp very closely, and hence the scattering appears to be independent of isospin. This

---

* The structure in the elastic proton-proton angular distributions summarised in subsect. 4.1 has been observed in a C I RN ISR experiment at equivalent conventional accelerator momenta up to 1500 GeV/c. These preliminary data, reported at the Batavia Conference in September 1972 by the Aachen-C I RN-Genoa-Harvard-Turin Group, show that the structure at $|t| \approx 1$ 2   1.5 GeV^2 becomes more pronounced as compared with the results of the present experiment. In addition, the energy dependence at fixed $|t|$ appears to slow down. These facts are compatible with the suggestion of the appearance of an asymptotic distribution as given by the papers of ref [30]

is, of course, consistent with the very small cross section [94] of pn charge-exchange scattering at high energy in the $|t|$ range where the process has been measured.

(iv) The overall energy dependence, at fixed $|t|$, in the region of the structure is rather strong up to 30 GeV/c, as may be seen in fig. 16. From the present data it is impossible to predict whether a limiting distribution in the structure region will be reached at much higher energies. This would necessitate the rapid flattening with energy of the steeply descending curves shown in fig. 16. A general feature of high-energy scattering appears to be that cross sections at fixed s are further from an asymptotic behaviour the larger the momentum transfer.

(v) The basic idea of Wu and Yang [29], concerning collisions at large momentum transfers and energies, that the pp elastic scattering differential cross section approaches the dependence of $G^4(t)$ is not contradicted by the data for $|t| \gtrsim 5$ GeV^2 at the highest energies shown in figs. 11 and 15. Of course, this rather tentative support of the Wu-Yang suggestion may be only fortuitous, particularly considering the comparatively low energies involved ($s \lesssim 50$ GeV^2). It is clear that experiments studying high momentum transfer scattering at much greater energies are needed to test these ideas rigorously. In the region of moderate momentum transfer ($|t| \sim 1$ GeV^2) the strong deviations from a $G^4(t)$ behaviour are expected on the basis of the optical models (subsect. 5.1.2) which also employ the electromagnetic form factor to determine the shape of the nuclear matter distribution.

As demonstrated in subsect. 5.1.2 the experimental features outlined above are not quantitatively explained by any single model or theoretical approach. It is only in the general or qualitative feature that the models have some measure of success. One of the most interesting of all of these models is that the structure is the first hint of an asymptotic or limiting distribution outside the main diffraction peak. The dynamical mechanism generating the scattering in this region has been described by the pomeron pole and cuts, by explicit multiple scattering models involving quarks or partons, and by the operation of a point-like interaction analogous to electromagnetism. The present data offer no possibility to distinguish between these alternatives even if the basic premise, namely that the structure is a limiting feature, is correct.

Another difficulty is the energy dependence for $|t| \gtrsim 1$ GeV^2. This, in the above terms, is generally considered to be made up from strongly energy-dependent contributions, particularly ordinary Regge pole and cuts. However, the quantitative formulation is very unsatisfactory and even the qualitative feature that the structure becomes apparent at a rather well-defined energy, around 8 GeV, is unexplained apart from the observation (see refs. [18, 23]) that baryon pair production comes into play in this energy region. It may be concluded that the basic idea that the structure is asymptotic can only be studied by pp experiments at higher energies or by searches for structure which develops with energy in the other hadronic systems. The discovery of such effects in, for example, πp scattering would provide considerable support for the idea of a common hadronic scattering mechanism at very high energies.

6.2 Inelastic scattering

The experimental facts obtained from the present experiment at 24.0 GeV/c support the known body of information outlined in subsect. 2.5 The new features emerging specifically concern large four-momentum transfers, beyond the forward peak, at $|t|$ values $\gtrsim 1$ GeV^2

(i) The similarity of the elastic, the N(1520) and the N(1688) distributions for $|t| \gtrsim 2$ GeV^2 strongly supports the idea of a common mechanism, for example multiple scattering, for the scattering process

(ii) While the elastic scattering distribution exhibits one rather well-defined structure around $|t| = 1.5$ GeV^2, the N(1520) and N(1688) cross sections are rather smooth. While there may be common dynamical mechanisms for both elastic and inelastic amplitudes in this region, the more complicated spin structure of the nucleon resonance amplitudes may cause a filling-in of the structure, a proposal which is commonly invoked in the elastic scattering with respect to various scalar model predictions

(iii) The production of the N(1400) has been explored, for the first time up to $|t| \simeq 1.5$ GeV^2 The suggestion of a structure in the angular distribution of fig. 20b should be viewed with caution, considering the difficulties involved in extracting the N(1400) cross sections, as discussed in the text.

(iv) The mass dependence of the angular distributions, either nucleon resonances or continuum states, is an interesting feature and may be compared with the behaviour of inelastic electron-proton scattering In the latter, dynamical importance is attached to the flattening of angular distributions at large missing mass Proton-proton reactions perhaps also reflect these features, in common with other hadronic processes However as the basic mechanism of hadronic interactions is much less clear-cut than the one photon processes of electroproduction, little can be said in this direction.

(v) Apart from the general features of diffraction dissociation and multiple scattering already discussed, the available theoretical discussions contribute little to quantitative considerations of the resonance production data, particularly at large $|t|$. The relationship between elastic and inelastic scattering appears to be more profitably discussed however

(vi) As a practical point it would appear difficult to pursue the *details* of the single resonance production reactions to much higher energies by missing mass experiments The available experimental mass resolutions rapidly become insufficient using present techniques

6.3 A final remark

Although the present experiment exhibits interesting features, as outlined above, of elastic or inelastic proton-proton scattering it seems clear that the elucidation of the dynamics can only result from experiments at higher energy and comparison

with other hadronic scattering systems. In addition more detailed work between 7 and 10 GeV/c, where the structure in the angular distribution develops would seem to be useful

References

[1] J.V. Allaby, F. Binon, A.N. Diddens, P. Duteil, A. Klovning, R. Meunier, J.P. Peigneux, F.J. Sacharidis, K. Schlupmann, M. Spighel, J.P. Stroot, A.M. Thorndike and A.M. Wetherell, Phys. Letters 28B (1968) 67.

[2] J.V. Allaby, A.N. Diddens, R.W. Dobinson, A. Klovning, J. Litt, L.S. Rochester, K. Schlupmann, A.M. Wetherell, U. Amaldi, R. Biancastelli, C. Bosio and G. Matthiae, Phys. Letters 34B (1971) 431

[3] U. Amaldi, R. Biancastelli, C. Bosio, G. Matthiae, J.V. Allaby, A.N. Diddens, R.W. Dobinson, A. Klovning, J. Litt, L.S. Rochester, K. Schlupmann and A.M. Wetherell, Phys. Letters 34B (1971) 435

[4] L. Van Hove, Rev. Mod. Phys. 36 (1964) 655

[5] A.N. Diddens, The differential cross section of proton-proton elastic scattering above 1 GeV, to be published in Landolt-Bornstein

[6] S. Fernbach, R. Serber and T.B. Taylor, Phys. Rev. 75 (1949) 1352

[7] G.G. Beznogikh, A. Buyak, K.I. Iovchev, L.I. Kirillova, P.K. Markov, B.A. Morozov, V.A. Nikitin, P.V. Nomokonov, M.G. Shafranova, V.A. Sviridov, Truong Bien, V.I. Zayachki, N.K. Zhidkov, T.S. Zoln, S.B. Nurushev, V.L. Solovianov, Phys. Letters 30B (1969) 274, G.G. Beznogikh, A. Bujak, L.I. Kirillova, B.A. Morozov, V.A. Nikitin, P.V. Nomokanov, A. Sandacz, M.G. Shafranova, V.A. Sviridov, Truong Bien, V.I. Zayachki, N.K. Zhidkov and T.S. Zoln, Phys. Letters 39B (1972) 411.

[8] U. Amaldi, R. Biancastelli, C. Bosio, G. Matthiae, J.V. Allaby, W. Bartel, G. Coccom, A.N. Diddens, R.W. Dobinson, V. Elings, J. Litt, L.S. Rochester and A.M. Wetherell, Phys. Letters 36B (1971) 504

[9] M. Holder, J. Radermacher, A. Staude, G. Barbiellini, P. Darriulat, M. Hansroul, S. Orito, P. Palazzi, A. Santroni, P. Strolin, K. Tittel, J. Pilcher, C. Rubbia, G. de Zorzi, M. Macri, G. Sette, C. Grosso-Pilcher, A. Lamberg and G. Maderni, Phys. Letters 35B (1971) 355, M. Holder, J. Radermacher, A. Staude, G. Barbiellini, P. Darriulat, P. Palazzi, A. Santroni, P. Strolin, K. Tittel, J. Pilcher, C. Rubbia, M. Bozzo, G. de Zorzi, M. Macri, S. Orito, G. Sette, A. Lamberg, C. Grosso-Pilcher and G. Maderni, Phys. Letters 36B (1971) 400, G. Barbiellini, M. Bozzo, P. Darriulat, G. Diambrini-Palazzi, G. de Zorzi, A. Lamberg, M.I. Ferrero, M. Holder, A. McFarland, G. Maderni, S. Orito, J. Pilcher, C. Rubbia, A. Santroni, G. Sette, A. Staude, P. Strolin and K. Tittel, Phys. Letters 39B (1972) 663

[10] R A Carrigan, Phys Rev. Letters 24 (1970) 168

[11] G. Cocconi, A N. Diddens, I . Lillethun, G Manning, A.I Taylor, T G Walker and A.M. Wetherell Phys Rev Letters 7 (1961) 450,
A N Diddens, I Lillethun, G Manning, A I Taylor, T G Walker and A.M Wetherell, Phys Rev Letters 9 (1962) 111

[12] G Cocconi, V T Cocconi, A D Krisch, J Orear, R Rubinstein, D.B. Scarl, W I Baker, I W Jenkins and A I . Read, Phys Rev Letters 11 (1963) 499 and Phys. Rev. 138 (1965) B165

[13] J Orear, Phys Letters 13 (1964) 190

[14] R Hagedorn, Nuovo Cimento Suppl 3 (1965) 147 (and other references contained in this paper)

[15] C M Ankenbrandt, A.R Clyde, B Cork D Keefe, I T. Kerth, W.A Layson and W.A. Wenzel, Nuovo Cimento 35 (1965) 1052.

[16] T. Ericson, CERN report TH 406 (1964),
T. Ericson and T. Mayer-Kuckuk, Ann. Rev. Nucl Sc. 16 (1966) 183

[17] J V. Allaby, G. Bellettini, G. Cocconi, A.N. Diddens, M.I Good, G Matthiae, I J. Sacharidis, A Silverman and A M. Wetherell, Phys. Letters 23 (1966) 389

[18] J V Allaby, G Cocconi, A.N. Diddens, A Klovning, G. Matthiae, I J Sacharidis and A M Wetherell, Phys Letters 25B (1967) 156

[19] C W Akerlof, R.H. Hieber, A.D Krisch, K.W. Edwards, L.G. Ratner and K. Ruddick, Phys. Rev. Letters 17 (1966) 1105 and Phys Rev. 159 (1967) 1138.

[20] J V Allaby, A.N. Diddens, A Klovning, F. Lillethun, I I Sacharidis, K. Schlupmann and A.M. Wetherell, Phys. Letters 27B (1968) 49

[21] G.D Kaiser, A review of models of the shape of the intermediate and large angle proton-proton elastic differential cross-section, report CTS-HE-69-3, Centre for Theoretical Studies, University of Miami, Coral Gables, Florida,
C B Chiu, Rev Mod Phys 41 (1969) 640,
J D. Jackson, Rev. Mod. Phys. 42 (1970) 12,
R.J Eden, Rev Mod. Phys. 43 (1971) 15

[22] S Frautschi, Ericson fluctuations and the Bohr model in hadron physics, CERN report TH-1463 (March 1972), to be published in Nuovo Cimento.

[23] J J L Kokkedee and L Van Hove, Phys. Letters 25B (1967) 228.

[24] A.D Krisch in Lectures in theoretical physics, ed. W.E. Brittin et al. vol IX. (University of Colorado Press, Boulder, Colorado, 1966)

[25] A D Krisch, Phys Rev. Letters 19 (1967) 1149,
M.M. Islam and J Rosen, Phys Rev 185 (1969) 1917 and references cited therein.

[26] J G Asbury, L G Ratner, A.I Read, D G Crabb, J.L. Day, A.D. Krisch, M.T. Lin and M.L Marshak, Phys Rev Letters 21 (1968) 1097,
M A. Abolins, G A Smith, Z Ming Ma, I Gellert and A B Wicklund, Phys Rev Letters 25 (1970) 126

[27] E Leader and M.R Pennington, Phys Rev Letters 27 (1971) 1325

[28] R Serber, Rev. Mod Phys 36 (1964) 649,
D. Weingarten, Phys Rev. D2 (1970) 201.

[29] T.T. Wu and C.N Yang, Phys. Rev 137 (1965) B708.

[30] T T Chou and C N. Yang, Proc Conf. on high energy physics and nuclear structure, Rehovoth, 1967 ed G. Alexander (North Holland, Amsterdam, 1967) p 348,
L Durand and R. Lipes, Phys Rev Letters 20 (1968) 637,
T T Chou and C.N. Yang, Phys Rev 170 (1968) 1591 and Phys. Rev Letters 20 (1968) 1213,
T Y. Cheng, S Y Chu and A.W Hendry, A unified picture of proton-proton elastic scattering at all angles from 3 to 24 GeV/c Indiana University preprint COO-2009-33 (1972).

[31] D R Harrington and A Pagnamenta, Phys Rev 173 (1968) 1599 and 184 (1969) 1908,
     F Shrauner, I Benoty and D W. Cho, Phys. Rev. 177 (1969) 2590 and 181 (1969) 1930.

[32] R.J Glauber, in Lectures in theoretical physics ed. W I Brittin et al , vol 1 (Interscience,
     New York, 1959) p. 315,
     R.J Glauber in High-energy physics and nuclear structure (North Holland, Amsterdam,
     1967) p 311

[33] G. Cocconi, Nuovo Cimento 57A (1968) 837

[34] W. Rarita, R J Riddel, C.B Chiu and R.J.N. Phillips, Phys. Rev. 165 (1968) 1615,
     D.M. Austin, W.H. Greiman and W. Rarita, Phys. Rev. 2 (1970) D2613

[35] A.A. Anselm and I.T. Dyatlov, Phys. Letters 24B (1967) 479.

[36] C.B. Chiu and J Finkelstein, Nuovo Cimento 57A (1968) 649 and 59A (1969) 92.

[37] S. Frautschi and B Margolis, Nuovo Cimento 56A (1968) 1155.

[38] M Greco, Phys Letters 31B (1970) 216

[39] G. Veneziano, Nuovo Cimento 57A (1968) 190.

[40] H.D.I. Abarbanel, S D Drell and F J. Gilman, Phys Rev. 177 (1969) 2458.

[41] F. Cerulus and A. Martin, Phys. Letters 8 (1964) 80.

[42] C.B. Chiu and C.I Tan, Phys. Rev 162 (1967) 1701,
     R.J Eden and C I. Tan, Phys Rev. 172 (1968) 1583

[43] T. Kinoshita, Phys. Rev. Letters 12 (1964) 257,
     A. Martin, Nuovo Cimento 37 (1965) 671.

[44] G.B Chadwick, G.B. Collins, C.L. Swartz, A. Roberts, S. de Benedetti, N.C. Hien and
     P J. Duke, Phys. Rev. Letters 4 (1960) 611,
     G B Chadwick, G.B. Collins, P.J. Duke, T. Fujii, N.C. Hien, M.A.R. Kemp and F. Turkot,
     Phys. Rev. 128 (1962) 1823.

[45] G. Cocconi, F. Fillethun, J.P. Scanlon, C.A. Ståhlbrandt, C.C. Ting, J. Walters and A.M
     Wetherell, Phys. Letters 8 (1964) 134.

[46] Particle Data Group, Rev Mod. Phys 43 (1971) 1.

[47] F.D. Roper, Phys. Rev Letters 12 (1964) 340.

[48] G Bellettini, G. Cocconi, A N Diddens, F Fillethun, J.P. Scanlon, A.M. Shapiro and
     A.M Wetherell, Phys Letters 18 (1965) 167

[49] F. Gellert, G A Smith, S. Wojcicki, E Colton, P.F. Schlein and H.K. Ticho, Phys. Rev.
     Letters 17 (1966) 884,
     R.A. Jesperson, Y.W. Kang, W.J Kernan, R.A. Leacock, J.I. Rhode, T.I Schalk and I.S.
     Schroeder, Phys. Rev. Letters 21 (1968) 1368.

[50] E W. Anderson, E J Bleser, G.B. Collins, T. Fujii, J. Menes, P. Turkot, R A. Carrigan, R.M
     Edelstein, N C. Hien, T.J McMahon and I Nadelhaft, Phys. Rev. Letters 16 (1966) 855,
     R.M. Edelstein, R A. Carrigan, N C Hien, T J McMahon, I Nadelhaft, E W Anderson,
     E J Bleser, G.B Collins, T. Fujii, J. Menes and F Turkot, Phys Rev. D5 (1972) 1073.

[51] I M. Blair, A.E. Taylor, W.S Chapman, P.I P. Kalmus, J Litt, M.C. Miller, H.J. Sherman,
     A. Astbury, D B. Scott and T.G Walker, Nuovo Cimento 63A (1969) 529.

[52] K.J. Foley, R.S. Jones, S.J Lindenbaum, W.A Love, S. Ozaki, E D. Platner, C.A. Quarles
     and F.H. Willen, Phys. Rev Letters 19 (1967) 397.

[53] C.M. Ankenbrandt, A.R. Clark, B. Cork, T. Elioff, L.T. Kerth and W.A Wenzel, Phys. Rev.
     170 (1968) 1223

[54] J V Allaby, I Binon, A N. Diddens, P. Duteil, A. Klovning, R Meunier, J P. Peigneux,
     F J. Sacharidis, K. Schlupmann, M Spighel, J.P. Stroot, A.M. Thorndike and A.M. Wetherell,
     Phys. Letters 28B (1968) 229.

[55] M. Good and W. Walker, Phys. Rev 120 (1960) 1857.

[56] D.R.O. Morrison, Phys Letters 22 (1966) 528, Phys. Rev. 165 (1968) 1699, and rapporteur's
     talk at the Kiev Conf. 1970, issued as CERN report D Ph.II/Phys 71-10 (1971).

[57] Y.N. Gribov, Yad Fiz 5 (1967) 197.

[58] S I. Drozdov, ZhTIF 28 (1955) 734, 28 (1955) 736, JETP (Sov Phys) 1 (1955) 591
1 (1955) 588,
F V Inopin, ZhI II 31 (1956) 901, II IP (Sov Phys) 4 (1957) 764,
J S Blair, Phys Rev. 115 (1959) 928

[59] B.T. Feld, Angular distribution in nucleon-nucleon quasi-elastic diffraction scattering,
CERN reports TH-178 and -193 (1961).

[60] B.T Feld and P.C M. York, An optical model for elastic and inelastic two-body processes
at high energy, MIT preprint 5330 (1966),
J G. Rushbrooke, Phys. Rev. 177 (1969) 2357

[61] T.T Chou and C.N. Yang, Phys Rev 175 (1968) 1832.

[62] A Rubenstein, Phys Rev 182 (1969) 1748,
M. Litzur, Phys. Rev Letters 27 (1971) 895

[63] A.P. Contogouris, S.C. Trautschi and How Sen Wong, Phys Rev 129 (1963) 974.

[64] S C. Trautschi, M. Gell-Mann and I Zachariasen, Phys Rev 126 (1962) 2204.

[65] B. Margolis and A. Rottstein, Nuovo Cimento 45A (1966) 1010.

[66] S. Trautschi and B. Margolis, Nuovo Cimento 57A (1968) 427.

[67] A.W. Hendry and J S Tretil, Phys Rev 184 (1969) 1680.

[68] U. Amaldi, R. Biancastelli, C. Bosio, G. Matthiae, J V. Allaby, A.N Diddens, R.W Dobinson,
A Klovning, J. Litt, I.S Rochester, K. Schlüpmann and A M. Wetherell, Nucl. Phys. 39B
(1972) 39.

[69] U. Amaldi, R Biancastelli, C. Bosio, G. Matthiae, J V. Allaby, A.N Diddens, R.W. Dobinson,
A Klovning, J. Litt, I.S. Rochester, K Schlupmann and A.M. Wetherell, Nuovo Cimento
Letters 4 (1972) 121.

[70] J.V. Allaby, A N Diddens, R.W. Dobinson, A. Klovning, J. Litt, L.S Rochester, K Schlup-
mann, A M. Wetherell, U. Amaldi, R. Biancastelli, C. Bosio and G Matthiae, Comparison
of momentum spectra of secondary particles produced in proton-proton collisions at
14 2, 19 2 and 24.0 GeV/c, paper to appear in the Proc of the 4th Int Conf. on high-
energy collisions, Oxford, April 1972

[71] L . Mazzone, Cibles a hydrogene liquide retroidies à l'helium au PS, CERN internal report
(unpublished) CERN/MPS-MU/II 70-1 (1970)

[72] J.B. Cumming, J. Hudis, A.M Poskanzer and S. Kauffmann, Phys Rev 128 (1962) 2392,
J.B. Cumming, Ann. Rev. Nucl Sc. 13 (1963) 261.

[73] G. Bellettini, G. Cocconi, A N Diddens, I . Lillethun, G Matthiae, J.P. Scanlon and A M.
Wetherell, Nucl. Phys 79 (1966) 609.

[74] E.W. Anderson, E.J. Bleser, H.R. Blieden, G B. Collins, D. Garelick, J Menes, I . Turkot,
D Birnbaum, R.M. Edelstein, N C Hien, T.J McMahon, J T. Mucci and J.S Russ, Phys.
Rev. Letters 25 (1970) 699.

[75] E.D Bloom, D H. Coward, H. De Staebler, J Drees, G. Miller, L.W Mo, R.E Taylor, M
Breidenbach, I I. Friedman, G.C Hartmann and H.W. Kendall, Phys Rev. Letters 23 (1969)
930,
M Breidenbach, Inelastic electron-proton scattering at high momentum transfer, Ph D
thesis MIT (1970),
G Miller, E.D Bloom, G Buschhorn, D.H Coward, H De Staebler, J Drees, C L Jordan,
L W. Mo, R.E. Taylor, J I. Friedman, G C Hartmann, H W. Kendall and R. Verdier, Phys
Rev. D5 (1972) 528.

[76] A.R Clyde, UCRL-16275 (1966)

[77] B.B Brabson, R.R Crittenden, R M Heinz, R C Kammerud, H.A Neal, H W. Paik, R.A
Sidwell and K.P Suen, Phys. Rev. Letters 23 (1969) 1306,
R.C. Kammerud, B.B. Brabson, R R. Crittenden, R M. Heinz, H A. Neal, H W. Paik and
R A. Sidwell, Phys. Rev D4 (1971) 1309.

[78] H. Palevsky, J.L. Friedes, R.J Sutter, G W. Bennett, G.J. Igo, W.D. Simpson, G.C Phillips,
D.M. Corley, N.S. Wall, R.L . Stearns and B Gottschalk, Brookhaven National Laboratory
report BNL 11360 (1967) unpublished.

[79] H Harari, Ann. of Phys. 63 (1971) 432.

[80] D. Birnbaum, R.M. Edelstein, N.C Hien, T.J McMahon, J.I Mucci, J.S. Russ, F W. Anderson, F.J. Bleser, H R. Blieden, G.B. Collins, D. Garelick, J. Menes and F Turkot, Phys. Rev. Letters 23 (1969) 663.

[81] M. Borghini, I . Dick, L di Lella, A. Navarro, J.C Olivier, K. Reibel, C. Coignet, D. Cronenberger, G Grégoire, K. Kuroda, A Michalowicz, M Poulet, D. Sillou, G Bellettini, P I Braccini, T. Del Prete, I . I oa, G Sanguinetti and M. Valdata, Phys Letters 31B (1970) 405.
M. Borghini, I Dick, J C Olivier, H Aoi, D. Cronenberger, G. Grégoire, Z. Janout, K. Kuroda, A. Michalowicz, M. Poulet, D. Sillou. G. Bellettini, P L. Braccini, T. Del Prete, L. I oa, P I aurelli, G. Sanguinetti and M. Valdata, Phys Letters 36B (1971) 501.

[82] L. Van Hove, Proc. Stony Brook Conf on high energy two-body reactions, April 1966 and in Particle interactions at high energies, Scottish Universities Summer School 1966, edited by T.W. Preist and I .L. Vick (Oliver and Boyd, 1967) p 63, sect. 4.4.

[83] R.A. Carrigan, R M. Edelstein, N C. Hien, T.J McMahon, I. Nadelhaft, I .W. Anderson, I .J. Bleser, G B Collins, T I upn, J Menes and I . Turkot, Phys. Rev. Letters 24 (1970) 683.
R.M. Edelstein et al., ref [50].

[84] K.J. Foley, S.J Lindenbaum, W.A. Love, S. Ozaki, J.J. Russell and L.C I . Yuan, Phys. Rev. Letters 11 (1963) 425,
K.J Foley, R.S. Gilmore, S.J. I indenbaum, W.A. Love, S. Ozaki, I .H Willen, R. Yamada and L C.I . Yuan, Phys. Rev. Letters 15 (1965) 45,
D. Harting, P Blackall, B Elsner, A.C . Helmholz, W.C. Middelkoop, B. Powell. B. Zacharov, P. Zanella, P Dalpiaz, M.N. Focacci, S. I ocardi, G. Giacomelli, L Monari, J A Beaney, R.A. Donald, P. Mason, L.W. Jones and D.O. Caldwell, Nuovo Cimento 38 (1965) 60,
J Orear. R. Rubinstein, D.B. Scarl, D.H. White, A D. Kirsch, W.R. I risken, A.L. Read and H. Ruderman, Phys. Rev. 152 (1966) 1162.

[85] O. Benary, I R. Price and G. Alexander (Particle Data Group), UCRL report 20000 NN (1970), p 84, and references cited therein.

[86] I W. Anderson et al , ref. [74].

[87] D.R.O Morrison, ref. [56]

[88] P G.O. I reund, Phys Rev. Letters 21 (1968) 1375.

[89] W.I I llis, R.R. Kinsey, T.W. Morris, R.S Panvini and F. Turkot, Phys Letters 32B (1970) 641.

[90] J.D. Bjorken, Phys. Rev 179 (1969) 1547.
J.V. Allaby, A.N. Diddens, A. Klovning, K Schlupmann and A.M. Wetherell, Phys. Letters 33B (1970) 429

[91] J M. Wang and I .I Wang, Phys. Rev. Letters 26 (1971) 1287,
P.D. Ting and H.J. Yesian, Phys. I etters 35B (1971) 321,
R.M I delstein, V Rittenberg and H.R. Rubinstein, Phys. Letters 35B (1971) 408,
J. Dias de Deus and W.S I am, Phys. Letters 38B (1972) 220, 38B (1972) 317,
M. Bishari and H J. Yesian, Phys Letters 38B (1972) 312

[92] J. Benecke, I.T. Chou, C.N. Yang and F. Yen, Phys. Rev. 188 (1969) 2159.

[93] I D Bloom and I J Gilman, Phys Rev I etters 25 (1970) 1140.

[94] J I ngler, K. Horn, I . Mönnig, P. Schludecker, W. Schmidt-Parzefall, H Schopper, P Sievers, H. Ullrich, R. Hartung, K. Runge and Yu. Galaktionov, Phys. Letters 34B (1971) 528